

## Article

# Heavy Metal Dispersion in a Hydrological Sub-Basin as Consequence of Mining Activity in Taxco, Guerrero (Southern Mexico)

Juan Carlos Ramírez-Javier <sup>1</sup>, Alejandro Hermelindo Ramírez-Guzmán <sup>2,\*</sup>, Giovanni Hernández-Flores <sup>3,\*</sup> , Mario Alberto Hernández Hernández <sup>4</sup> , Oscar Talavera-Mendoza <sup>2</sup>, Sergio Adrián Salgado Souto <sup>2</sup> and Alejandra Cortés-Silva <sup>5</sup>

<sup>1</sup> Facultad de Ecología Marina, Universidad Autónoma de Guerrero, Av. Gran Vía Tropical No. 20, Fracc. Las Playas, Acapulco 39390, Mexico

<sup>2</sup> Escuela Superior de Ciencias de la Tierra, Universidad Autónoma de Guerrero, Ex hacienda de San Juan Bautista s/n, Taxco de Alarcón 40323, Mexico

<sup>3</sup> CONACYT-Escuela Superior de Ciencias de la Tierra, Universidad Autónoma de Guerrero, Ex Hacienda San Juan Bautista s/n, Taxco de Alarcón 40323, Mexico

<sup>4</sup> CONACYT-Instituto de Geofísica, Universidad Nacional Autónoma de México, Ciudad Universitaria, Delegación Coyoacán, Ciudad de México 04510, Mexico

<sup>5</sup> Instituto de Geofísica, Universidad Nacional Autónoma de México, Ciudad Universitaria, Delegación Coyoacán, Ciudad de México 04510, Mexico

\* Correspondence: halessandro2@hotmail.com (A.H.R.-G.); gherandez@conacyt.mx (G.H.-F.)

**Abstract:** The mining industry generates high concentrations of heavy metals (HMs) susceptible to being released into surface and ground water. The objective of this work was to determine the concentration and dispersion of HMs in surface water and ground water in a hydrological sub-basin located in southwest Mexico. The samples were collected as following: 24 samples from streams, rivers, and one lake, and 15 samples from springs, located along the Taxco-Cocula sub-basin. A total of 78 samples were collected in the dry and rainy seasons. Physicochemical parameters, major ions, and HMs were analyzed. The pH, Eh, electrical conductivity, and total dissolved solids were analyzed in situ, while the concentrations of anions, cations, and HMs were measured in the laboratory. The results were treated with multivariate analysis and PHREEQC simulation. The highest recorded values (in mg/L) were in surface water, where the HMs in the dry season were Al (28.63), As (0.60), Cd (1.78), Cu (1.10), Fe (68.27), Mn (21.47), Pb (0.02), and Zn (208.80). These high concentrations exceed the limits established by national and international regulations for drinking water. The ground water did not indicate pollutants associated to the mining industry. On the other hand, in the rainy season, the surface water showed a decrease in the concentrations of the measured heavy metals. The hypsometric gradient and the hydrogeological and meteorological characteristics of the Taxco-Cocula sub-basin are the factors that contribute to the dilution and dispersion of the HMs along the 60 km of its length.

**Keywords:** ground water; hydrogeochemistry; mining waste; surface water; Taxco mining district; water quality



**Citation:** Ramírez-Javier, J.C.; Ramírez-Guzmán, A.H.; Hernández-Flores, G.; Hernández Hernández, M.A.; Talavera-Mendoza, O.; Salgado Souto, S.A.; Cortés-Silva, A. Heavy Metal Dispersion in a Hydrological Sub-Basin as Consequence of Mining Activity in Taxco, Guerrero (Southern Mexico). *Water* **2023**, *15*, 1950. <https://doi.org/10.3390/w15101950>

Academic Editor: Lahcen Zouhri

Received: 4 April 2023

Revised: 28 April 2023

Accepted: 18 May 2023

Published: 21 May 2023



**Copyright:** © 2023 by the authors. Licensee MDPI, Basel, Switzerland. This article is an open access article distributed under the terms and conditions of the Creative Commons Attribution (CC BY) license (<https://creativecommons.org/licenses/by/4.0/>).

## 1. Introduction

Mining activity is an essential activity around the world. However, it is also an important source of hazardous pollutants, such as heavy metals (HMs), Pb, Cd, As, Sb, Cr, and Zn among others, which are non-biodegradable and difficult to remove. These pollutants can be incorporated into natural resources, such as water, soil, air, flora, and fauna [1–4]. Water plays a key role in the dispersion of HMs. It is considered to be a “transporting agent”, one of the most effective ways to disperse dissolved or non-dissolved materials in surface and ground water [5]. Through consumption of contaminated water in the food chain,

HMs can enter humans, where they are responsible for serious diseases, such as cancer [6]. Therefore, HMs have become environmental and food safety concerns [7]. The presence of, and dispersal mechanisms of, HMs must be documented, taking into consideration spatial and temporal distributions, in addition to their possible impact on ground water used as drinking water sources supplying towns.

The Taxco Mining District (TMD) is located in southwest Mexico, wherein mining has developed since five centuries ago (Figure 1). Gold and silver are the main metals extracted from the region [8]. However, the mines of TMD are distributed along the main recharge zone of the hydrological Taxco-Cocula sub-basin in the state of Guerrero. As a consequence of the mining, there are seven tailing dams in the Taxco region, which represent ca. 55 million tons of mining waste [9,10]. These leachate impoundments are located on riverbanks and ravines, facilitating dispersion of the HMs and their incorporation into water, air, and soil. Moreover, pyrite is one of the main sulfur minerals found in tailings, and its natural oxidation produces acid mine drainage (AMD), an acidic and hazardous effluent with high HM concentration that contributes to HM dispersion by infiltration or by surface water pollution [11]. Furthermore, in the Taxco region, there are small localities where mining activity has been practiced, which contribute to HM dispersion.

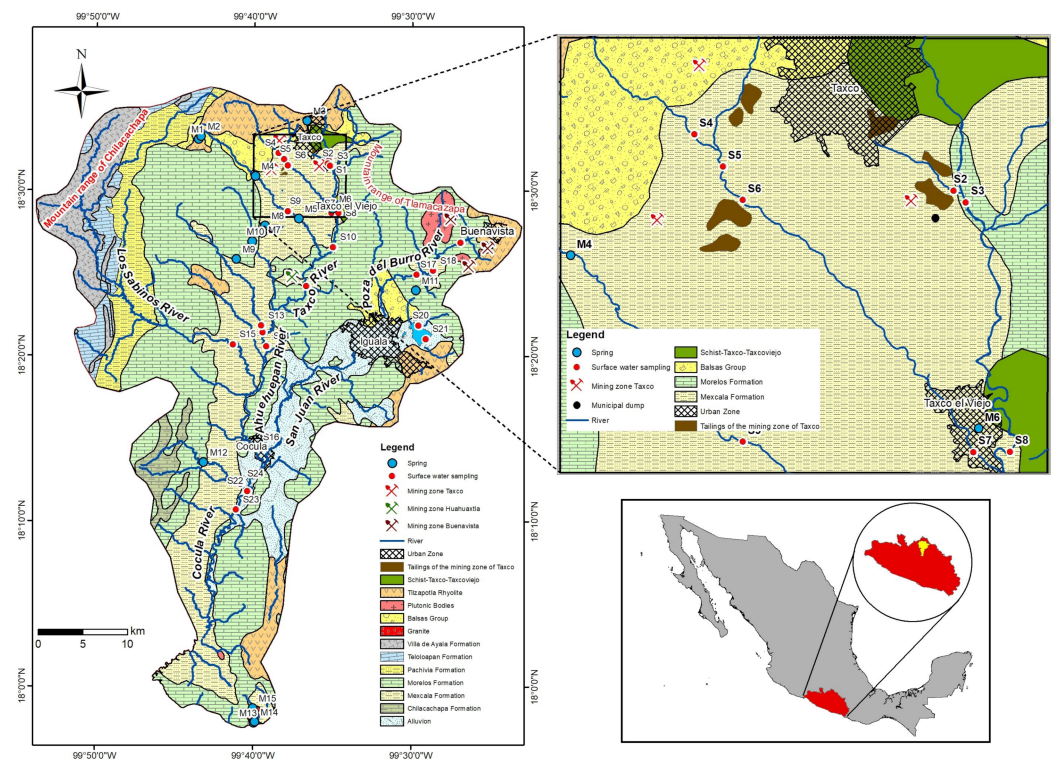


**Figure 1.** Location and surface area of the Taxco-Cocula sub-basin and Mining area of Taxco. Sampling sites and location of tailings.

Previous research, carried out in the recharge zone of the hydrological Taxco-Cocula sub-basin, showed that the water quality from the tributary streams of the Taxco and Cacalotenango rivers was not fit for human consumption, due to high contents of Pb and other HMs [3,12,13]. Despite this finding, surface water in the hydrological Taxco-Cocula sub-basin is the main water source for the population in both seasons. On the other hand, Ramirez Javier [14] evaluated concentrations of HMs in ground water near the recharge areas in the hydrological Taxco-Cocula sub-basin and found the concentrations of HMs did not exceed the permissible limits of national and international standards for water for human consumption, NOM-127-SSA1-2021, and the World Health Organization (WHO) standards [15,16].

Although the quality of surface and ground water in the upper part of the hydrological Taxco-Cocula sub-basin has been researched, the environmental impact caused by the dispersion of HMs in the middle and lower parts of the hydrological Taxco-Cocula sub-basin has not been studied. The focus of the research presented herein was on analyzing the concentration and distribution of HMs through the hydrological Taxco-Cocula sub-basin, so as to evaluate the current situation of water resources (surface and ground) beyond the mining influence, with the help of hydrogeochemical tools and multivariate analysis.

## 2. Materials and Methods

### 2.1. Overview of the Study Area

Figure 1 shows the study area, the hydrological Taxco-Cocula sub-basin, located in southwest Mexico and in the northern region of the state of Guerrero ( $17^{\circ}57'41''$  and  $18^{\circ}36'05''$  latitude north and  $99^{\circ}22'39''$  and  $99^{\circ}53'27''$  longitude east).

Two lithological groups emerge within the hydrological Taxco-Cocula sub-basin: the Guerrero-Morelos Platform (GMP) and the Guerrero Terrain (GT) [17,18]. The GMP sedimentary cover has wide distribution (over ~90% of the area) along the sub-basin (Figure 1). Metamorphic rocks, called Schist Taxco and Roca Verde Taxco Viejo, of Valanginian age emerge to the north [17]. These rocks present intense fracturing and faulting, which confer an aquitard function with springs, with a flow rate of  $Q = 0.012\text{--}0.016$  L/s. In the study area, there are also rocks composed of clay carbonate rocks of the Chilacachapa Formation from the Aptian–Albian age [19], and limestones of the Morelos Formation from the Albian–Cenomanian age [20], having a discharge flow rate of 20 L/s in some springs. At the sandy horizons of the Mezcala Formation, of the Cenomanian–Maastrichtian early age [21], there are terrigenous marine rocks, with a flow rate in the order of 0.012–0.016 L/s. In springs to the north, and in the central part, there is a continental sedimentary sequence called the Balsas Group from the Paleocene–Eocene age [22], having extraction rates of 2–36 L/s in springs. To the north, and overlaying the stratigraphic column, extrusive igneous rocks emerge, named Rhyolite Tilzapotla, from the Eocene age [18], and these rocks function as aquifuges in the region. To the east of the area, granodioritic plutonic bodies are observed [8]. To the northwest, there is a GT arc sequence that has a distribution within the sub-basin of ~10% (Figure 1), covered with metamorphic rocks from the Villa de Ayala Formation from the Berrasian–Aptian age, limestone with volcanic influence from the Teloloapan Formation from the Late Aptian–Late Albian age and terrigenous marine rocks of the Pachivia Formation from the Cenomanian–Turanian age [23].

The study area was the middle basin of the Balsas River, in the 18th Hydrological Region and the Administrative Region IV Balsas, considered one of the largest hydrological basins of the Mexican Republic [24]. The hydrological sub-basin of the Taxco-Cocula River is subdivided into smaller catchments that make up the main tributary system (Figure 1). The sub-basin is ~80 km long and the runoffs begin in the Sierra de Taxco, at an altitude of 2700 masl with the Taxco River. Later, the river's name changes to the Cocula River, which ends at the hydroelectric dam Ing. Carlos Ramírez Ulloa at 450 masl (Figure 1). Throughout the hydrological sub-basin, the Taxco-Cocula River is intercepted by a large number of streams, such as the Xochula, Cacalotenango, Poza del Burro, Temixco, and the Los Sabinos river, among other smaller streams (Figure 1).

The geology of the region establishes the configuration of the surface runoffs, like the marine terrigenous rocks of the Mezcala Formation, which act as an impermeable unit influencing the preferential north–south direction of the Taxco-Cocula River runoff. The maximum altitudes and the behavior of precipitation suggest that the recharge zone, and the beginning of surface runoff, take place mainly in the Sierra de Taxco. In addition, a system of lateral flows originates in the topographic highlands that border the sub-basin (e.g., to the east, the Sierra de Tlamacazapa, and, to the west, the Sierra de Chilacachapa). The climate in the study area is warm and subhumid, with rainfall from June to October. There is an average annual rain of 1100 mm. June, August, and September are the months

of greatest rain intensity. After November there is a considerable drop in precipitation. Maximum dry conditions are recorded in the months of February to May [25].

In Mexico, the TMD has been the most important mining area, recognized for its exploitation of base metals (Cu, Pb, and Zn) and precious metals (Ag and Au) since 1522 [26]. The veins and mantles relate to metallic sulfides associated with minerals, such as pyrite, sphalerite, galena, chalcopyrite, argentite, native silver, polyblastite, proustite, and pyrargyrite [9]. The mineralized zones and mines of the region are in the mountainous zone, which is considered to be the recharge area (Figure 1).

The TMD is exploited by seven mining works [27], located 8 km southeast of Taxco city (Figure 1). The wastes from their activities have generated ~55 million tons of tailings, with a particle size <40  $\mu\text{m}$  [9,28].

Mercury was extracted between 1948 and 1962 in four extraction sites close to the town of Huahuaxtla, located ~12 km to the south of Taxco de Alarcón in the medium part of the sub-basin (Figure 1). Gallagher and Pérez-Siliceo [29] reported elemental Hg ore and mineral species, such as: cinnabar, metacinnabar, calomel, terlinguaite, montroydite, and englestoneite. The mining tailings that originated in Huahuaxtla were produced by crushing and calcining limestone rock, without the intervention of other metallurgical separation processes, so the related waste had the size of gravel, with an accumulation of ~30.5 tons. However, this volume only represents  $5 \times 10^{-6}\%$  of the total volume extracted in the TMD. The deposits do not show evidence of oxidation and, so far, there is no evidence of AMD generation, due to the low existence of sulfides.

The Buenavista de Cuellar mining area (BCMA) is characterized by a skarn-type iron oxide deposit in limestone rocks of the Morelos Formation, related to granodioritic plutonic bodies [30], and located to the north-northeast in the upper part of the sub-basin (Figure 1). In the BCMA, iron is exploited intermittently by open-pit mining, presenting a mineral association with magnetite, hematite, and limonite, and, thus, the HM related to this area is Fe. At present, stone and marble materials are extracted from this area.

## 2.2. Sampling Description and Analysis

There were two sampling periods, with a total of 78 samples collected within the hydrological sub-basin (Figure 1). The first period was carried out during the dry season (December), while the second was in the rainy season (June). In each period, 24 surface water samples were taken, with sampling points located on the Taxco-Cocula River (S1, S2, S8, S10, S11, S12, S14, S16, S22, and S23), Los Sabinos River (S15), and Poza del Burro stream (S17, S18, and 19). Other samples were taken from the following tributary streams: Xochula (S2), Cacalotenango (S4, S5, S6, and S7), Temixco (S9), El Sabinito (S13), and Machito de las Flores (S24). Finally, two more samples were taken from Lake Tuxpan (S20 and S21) (Figure 1). Ground water samples were taken from 15 different spring discharges (M1–M15).

The water samples were collected according to APHA [31] guidelines. The water samples were carefully sampled, avoiding sediments or any particles. At each sampling point, a total volume of 1.5 L of water was collected and divided into two Nalgene™ high-density polypropylene bottles, sized 1000 and 500 mL. The bottles were subjected to pre-treatment, by being washed with dilute  $\text{HNO}_3$  (8 N) and deionized water. Aliquots of 1000 mL were refrigerated at 4 °C and used for anion analyses, while water samples of 500 mL were acidified with 2.5 mL of ultra-pure concentrated  $\text{HNO}_3$  (Ultrex II), filtered with cellulose nitrate filters, with a pore size of 0.45  $\mu\text{m}$ , and refrigerated at 4 °C. The acidified samples were used to determine the concentration of major cations and HMs. Electrical conductivity (EC), total dissolved solids (TDS), pH, and redox potential (Eh) were measured in situ. The EC, TDS, and pH were determined with a potentiometer, brand EUTECH model PCSTester 35, previously calibrated with the corresponding solutions. The Eh was determined using HANNA brand equipment, model HI 98201, previously calibrated with a Zobell solution.

### 2.3. Hydrochemical Analysis

From the 1000 mL samples, the concentrations of the following anions were determined: carbonates ( $\text{CO}_3^{2-}$ ), bicarbonates ( $\text{HCO}_3^-$ ), chlorides ( $\text{Cl}^-$ ), sulfates ( $\text{SO}_4^{2-}$ ), and nitrates ( $\text{NO}_3^-$ ). The  $\text{CO}_3^{2-}$  and  $\text{HCO}_3^-$  concentrations were determined by alkalinity and measured by titration, using hydrochloric acid (HCl 0.02 N) as the titrant, and phenolphthalein, bromocresol green, and methyl red as colorimetric indicators. The  $\text{Cl}^-$  concentration was determined by titration, using  $\text{AgNO}_3$  0.02 M as the titrant and  $\text{K}_2\text{CrO}_4$  0.041 M and phenolphthalein as colorimetric indicators. The  $\text{SO}_4^{2-}$  and  $\text{NO}_3^-$  concentrations were determined by colorimetry, using a colorimeter HACH DR/890.  $\text{BaCl}_2$  and cadmium reducing reagents were used for the determination of sulfates and nitrates, respectively.

The HM (Al, As, Ba, Cd, Co, Cr, Cu, Fe, Mn, Pb, Sr, V, and Zn) and major cation ( $\text{Ca}^{2+}$ ,  $\text{K}^+$ , and  $\text{Mg}^{2+}$ ) concentrations were determined by inductively coupled plasma-atomic emission spectroscopy (ICP–AES), using a Perkin Elmer (Waltham, USA) Optima 3200 DV. The precision was controlled by the repeated measurement of a sample and the accuracy by the measurement of the two standards after the analysis of 5 samples. Four High-Purity Certified Standards of water were used for calibration and a different one for accuracy. The lowest measured concentrations for each metal (mg/L) were as follows: Ag and Cd, 0.005; Ba, As, Pb, Se, Mo, and Sb, 0.010; Fe, Mn, Co, and Cu, 0.025. These values were considered the true detection limit (DL) of the instrument in the analyzed samples. The reported DL was determined following the procedure outlined by Talavera Mendoza et al. [9], who reported DL as the lowest concentration of an element that the instrument can accurately determine according to a certified standard. The  $\text{Na}^+$  was determined by Flame Atomic Absorption Spectroscopy (FAAS) (Perkin Elmer, Waltham, USA), using a Perkin Elmer Analyst 100 device.

A piper diagram was used to define the hydrochemical groups of the ground water from springs represented in this work, using Aquachem 4.0 software (Hydrogeologic, 1999). The Pearson correlation coefficient ( $r$ ), between the physicochemical parameters, major ions, and HM, was calculated with Excel, using a value of  $p < 0.05$ . The Principal Component Analysis (PCA), using the Varimax Rotation method, was carried out using Statistica 10 software (10.0.1011.6), to ascertain the groups formed according to the water–rock tailings interaction processes. To examine the saturation states that controlled the probable relationships between minerals, PHREEQC software was used, with equilibrium models from the WATEQ4F database [32].

## 3. Results

### 3.1. Physicochemical Parameters in Surface Water and Springs

Tables 1 and 2 provide the physicochemical characteristics of the surface water samples (S1 to S24) for dry and rainy seasons, respectively. Table 3 shows the physicochemical characteristics of the ground water samples (M1 to M15). In the dry season, the EC for surface water samples showed a median of 509.0  $\mu\text{S}/\text{cm}$  (Figure 2a), whereas in the rainy season it was 423.5  $\mu\text{S}/\text{cm}$ . In contrast, the measured EC median values recorded in the springs were 538.0 and 560.0  $\mu\text{S}/\text{cm}$  for the dry and rainy seasons, respectively. The TDS in the surface water for the dry season registered a median value of 392 mg/L and for the rainy season the observed value was 301.5 mg/L (Figure 2b). In the case of springs, for the dry season the median value was 381 mg/L, whereas 398 mg/L was recorded in the rainy season. The pH median values for surface water were 8.6 and 9.0 for the dry and rainy seasons. Regarding the springs, the pH determined in the dry season had a median value of 7.3, and of 7.27 in the rainy season, showing that there was no significant difference in this parameter between the two sampling periods (Figure 2c). The Eh recorded for surface water in the dry season had a median value of 160.4 and 121.7 mV in the rainy season. Sample S3 showed a remarkable difference in Eh between seasons (Tables 1 and 2). For spring water samples, the Eh for the dry season had a median value of 168.3 and was 128.6 mV for the rainy season (Figure 2d). The recorded results showed the samples located in the northern portion of the sub-basin stood out. Sample S2, for example, showed the

highest values recorded for EC, TDS, and Eh, these being 3530  $\mu\text{S}/\text{cm}$ , 2520  $\text{mg}/\text{L}$ , and 458.7  $\text{mV}$ , respectively, in the dry season. At the same sampling site, the pH was the most acidic measured in the entire sub-basin, with a value of 2.9 (Table 1).

**Table 1.** Physicochemical characteristics, major and minor ion concentrations from surface water: Dry season.

Sample	EC	TDS	pH	Eh	HCO <sub>3</sub> <sup>-</sup>	SO <sub>4</sub> <sup>2-</sup>	Cl <sup>-</sup>	NO <sub>3</sub> <sup>-</sup>	Ca <sup>2+</sup>	Na <sup>+</sup>	K <sup>+</sup>	Mg <sup>2+</sup>	SiO <sub>2</sub>
	$\mu\text{S}/\text{cm}$	$\text{mg}/\text{L}$	NA	$\text{mV}$	$\text{mg}/\text{L}$								
S1	1074	759	8.4	148.9	412.4	136	66.7	105.4	62.1	74.5	10.1	8.4	25.4
S2	3530	2520	2.9	458.7	0	2600	0.0	125.0	153.2	22.1	1.8	102.1	18.7
S3	1143	818	7.6	-65.4	300.1	230	65.8	95.5	68.3	79.1	10.8	14.0	26.9
S4	237	167	8.8	192.0	129.3	10	<DL	4.4	27.9	5.2	1.2	1.6	21.9
S5	312	162	8.9	152.0	153.7	26	<DL	1.4	30.0	4.8	1.1	2.0	18.0
S6	377	264	8.8	149.9	163.5	58	3.3	1.7	76.7	7.0	2.7	7.3	38.4
S7	594	422	8.4	192.2	209.8	120	5.8	2.5	143.5	9.3	3.1	13.8	37.4
S8	1130	803	8.3	192.2	197.6	200	63.3	85.7	183.5	65.3	19.0	33.1	43.3
S9	412	294	8.7	168.0	222.0	18	6.7	2.9	113.3	17.6	1.1	5.6	24.4
S10	584	828	8.5	247.1	173.2	200	24.2	25.8	150.4	29.5	7.6	23.3	38.3
S11	687	486	8.8	270.5	173.2	190	15.8	12.9	144.6	17.7	4.8	21.3	28.6
S12	383	540	9.0	167.4	153.7	200	17.5	11.9	151.5	19.6	5.8	25.5	24.6
S13	355	252	8.7	79.4	190.3	12	9.2	2.6	86.3	6.8	0.9	9.7	20.1
S14	684	489	9.5	111.2	190.3	120	11.7	6.7	126.4	12.8	3.0	17.6	23.5
S15	506	362	8.5	62.3	236.7	22	22.5	4.1	125.7	14.1	3.0	12.5	21.0
S16	447	315	8.8	161.9	197.6	34	22.5	7.4	102.8	14.8	3.0	13.9	21.9
S17	680	482	8.4	176.7	302.6	110	17.5	9.0	183.1	14.7	5.3	18.4	32.7
S18	651	461	7.8	184.7	283.0	86	28.3	1.5	162.5	18.5	9.2	18.4	33.4
S19	896	630	8.1	167.7	297.7	29	90.0	93.2	87.4	76.1	37.2	15.9	48.9
S20	443	314	8.2	78.8	178.1	61	10.8	1.4	55.9	41.8	11.1	15.6	9.7
S21	443	318	9.1	68.2	175.7	62	11.7	1.1	55.4	16.1	10.8	15.4	6.8
S22	510	235	8.9	158.9	231.8	41	20.0	9.7	110.8	16.1	4.1	13.6	23.9
S23	508	358	9.0	105.9	231.8	44	20.0	9.0	108.1	17.1	3.9	13.2	23.5
S24	425	303	8.4	155.9	209.8	20	3.3	3.8	95.9	4.1	1.1	16.7	22.5
<b>Values established by the World Health Organization</b>													
	NC	1000	7–8	NC	NC	250	250	50	75	200	NC	30	NC

EC: Electrical conductivity; TDS: Total dissolved solids; Eh: Redox potential; NA: Not applicable; DL: Detection limit; NC: Not considered by the World Health organization.

**Table 2.** Physicochemical characteristics, major and minor ion concentrations from surface water: Rainy season.

Sample	EC	TDS	pH	Eh	HCO <sub>3</sub> <sup>-</sup>	SO <sub>4</sub> <sup>2-</sup>	Cl <sup>-</sup>	NO <sub>3</sub> <sup>-</sup>	Ca <sup>2+</sup>	Na <sup>+</sup>	K <sup>+</sup>	Mg <sup>2+</sup>	SiO <sub>2</sub>
	$\mu\text{S}/\text{cm}$	$\text{mg}/\text{L}$	NA	$\text{mV}$	$\text{mg}/\text{L}$								
S1	385	271	8.53	153.3	109.8	76	14.0	19.4	34.6	16.5	2.7	3.9	19.5
S2	1122	792	8.51	225.3	256.2	460	21.0	19.77	153.9	20.2	2.4	19.1	14.5
S3	433	307	8.46	136.5	114.7	96	14.0	19.9	97.3	17.2	6.6	11.8	47.4
S4	254	181	9.37	119.4	139.1	12	2.0	1.55	42.4	5.6	1.5	2.7	28.4
S5	337	240	9.57	123.2	170.8	31	3.0	2.63	23.8	7.5	0.3	1.7	11.9
S6	374	266	9.60	122.1	180.6	47	2.0	2.17	92.9	7.9	2.3	7.9	41.6
S7	480	343	9.28	136.5	231.8	62	6.0	9.41	121.4	9.3	2.2	11.1	38.9
S8	406	289	8.42	138.0	151.3	76	10.0	14.32	96.3	12.1	4.5	10.3	41.4
S9	396	281	8.81	174.8	202.5	17	2.0	4.28	137.6	4.4	0.6	6.0	24.1
S10	580	411	9.25	129.0	253.8	86	15.0	14.46	135.3	15.3	3.3	12.9	35.6
S11	472	334	9.16	118.1	239.1	46	15.0	9.51	115.4	9.2	1.4	8.5	27.1
S12	477	337	9.52	109.2	228.6	64	10.0	11.89	80.5	9.1	1.4	7.2	20.1
S13	289	205	9.09	120.0	383.1	10	4.0	6.1	103.5	3.9	1.1	9.7	22.5
S14	426	303	9.41	113.1	209.8	49	9.0	6.73	88.5	11.5	2.2	7.7	22.5
S15	467	330	8.82	121.1	212.3	25	5.0	6.94	170.1	6.0	1.5	14.6	28.2

**Table 2.** *Cont.*

Sample	EC	TDS	pH	Eh	HCO <sub>3</sub> <sup>-</sup>	SO <sub>4</sub> <sup>2-</sup>	Cl <sup>-</sup>	NO <sub>3</sub> <sup>-</sup>	Ca <sup>2+</sup>	Na <sup>+</sup>	K <sup>+</sup>	Mg <sup>2+</sup>	SiO <sub>2</sub>
	μS/cm	mg/L	NA	mV	mg/L								
S16	416	296	8.85	119.4	200.1	31	4.0	6.61	134.9	6.8	1.5	12.5	26.5
S17	594	419	8.92	94.5	270.8	70	18.0	18	137.6	16.5	4.6	13.7	39.0
S18	510	360	9.08	135.2	229.4	67	18.0	11.89	99.4	17.8	5.9	11.0	35.4
S19	543	384	8.52	126.5	175.7	33	53.0	27.2	59.9	40.3	21.9	11.4	39.0
S20	417	296	10.00	121.3	163.5	74	13.0	0.54	38.3	49.4	10.9	12.7	9.2
S21	429	304	9.80	68.4	165.9	74	15.0	0.73	37.5	46.9	11.3	13.0	7.6
S22	375	266	8.93	97.3	190.3	28	5.0	8.5	105.5	7.4	2.0	10.1	21.7
S23	421	300	8.92	192.6	219.6	36	8.0	10.15	98.1	5.5	1.7	8.9	18.3
S24	304	216	8.81	106.3	146.4	17	<DL	10.06	79.5	2.1	1.2	7.8	14.5

**Values established by the World Health Organization**

NC	1000	7–8	NC	NC	250	250	50	75	200	NC	30	NC
----	------	-----	----	----	-----	-----	----	----	-----	----	----	----

EC: Electrical conductivity; TDS: Total dissolved solids; Eh: Redox potential; NA: Not applicable; DL: Detection limit; NC: Not considered by the World Health organization.

**Table 3.** Physicochemical characteristics, major and minor ion concentrations from ground water samples.

Sample	EC	TDS	pH	Eh	HCO <sub>3</sub> <sup>-</sup>	SO <sub>4</sub> <sup>2-</sup>	Cl <sup>-</sup>	NO <sub>3</sub> <sup>-</sup>	Ca <sup>2+</sup>	Na <sup>+</sup>	K <sup>+</sup>	Mg <sup>2+</sup>	SiO <sub>2</sub>
	μS/cm	mg/L	NA	mV	mg/L								
<b>Dry season</b>													
M1	40	21	7.38	179.8	54.2	1	<DL	1.0	13.2	5.5	2.8	0.418	44.1
M2	41	19	7.08	168.3	29.3	1	<DL	0.7	5.0	2.8	3.2	0.808	70.6
M3	83	42	6.65	223.2	61.0	<DL	<DL	0.3	10.8	8.5	2.5	0.183	74.0
M4	382	270	8.51	160.4	315.2	6	5.8	1.0	92.0	4.6	0.8	2.687	18.8
M5	401	285	8.03	149.5	229.4	20	5.0	1.4	82.6	6.3	0.8	4.174	19.7
M6	1062	736	7.06	172.5	392.8	120	54.2	57.7	213.2	15.7	1.0	12.85	23.7
M7	718	502	7.18	166.0	361.1	61	16.7	39.2	147.6	10.5	0.7	6.043	27.3
M8	632	470	6.87	159.2	621.2	6	5.0	4.3	183.3	3.0	0.2	1.689	12.3
M9	538	381	7.30	123.0	425.0	<DL	<DL	1.5	147.1	1.1	0.2	2.905	9.5
M10	593	420	7.40	171.9	465.0	<DL	<DL	0.7	163.2	1.4	0.2	3.658	11.4
M11	670	481	7.33	188.6	468.5	5	2.5	8.5	112.2	2.8	0.8	24.64	10.9
M12	448	318	8.50	145.5	229.4	17	1.7	5.8	66.1	2.2	0.9	14.86	12.9
M13	2264	1135	7.03	249.3	268.4	1000	26.7	1.0	352.2	16.5	1.8	76.42	16.8
M14	2039	1016	6.85	153.2	260.8	850	26.7	1.0	312.2	15.6	1.6	52.07	15.1
M15	532	266	7.60	187.3	243.3	68	3.3	10.2	51.8	17.9	2.2	20.56	28.6

**Rainy season**

M1	49	35	6.63	126.2	45.0	<DL	<DL	0	9.4	4.9	2.6	0.4	40.6
M2	52	37	7.52	117.9	29.3	1	<DL	0	4.9	2.5	3.1	0.8	64.7
M3	102	73	7.00	166.0	63.4	<DL	<DL	0	11.5	9.1	2.7	0.2	70.0
M4	422	300	8.88	79.8	275.7	5	2.0	2.26	94.0	3.3	0.6	2.3	14.9
M5	407	289	7.94	133.7	224.5	18	3.0	1.98	77.9	4.9	0.6	3.8	16.7
M6	777	550	6.97	185.3	263.5	98	26.0	39.22	137.2	18.3	0.7	7.5	21.9
M7	776	551	7.27	134.3	361.1	62	24.0	24.14	159.8	11.1	0.9	6.8	29.1
M8	630	446	7.03	110.3	407.5	3	3.0	1.84	123.5	1.9	0.1	1.0	8.0
M9	563	399	7.27	132.0	285.0	2	<DL	0.32	82.3	1.0	0.1	1.3	4.8
M10	560	397	7.36	112.7	300.0	1	<DL	2.8	83.9	1.1	0.1	4.2	6.6
M11	640	454	7.54	192.3	407.5	7	4.0	10.16	114.5	3.2	1.3	20.6	11.0
M12	452	320	8.70	114.0	135.0	15	0.0	7.73	42.1	2.0	0.2	2.0	4.0
M13	1945	1380	7.08	113.8	261.1	900	31.0	0.11	390.5	16.6	1.7	72.9	22.0
M14	1830	1290	7.12	131.0	258.6	800	28.0	0.9	310.7	16.2	1.4	53.1	17.2
M15	550	391	8.40	163.7	226.9	64	5.0	10.23	54.5	17.4	4.3	24.7	47.7

**Values established by the World Health Organization**

NC	1000	7–8	NC	NC	250	250	50	75	200	NC	30	NC
----	------	-----	----	----	-----	-----	----	----	-----	----	----	----

EC: Electrical conductivity; TDS: Total dissolved solids; Eh: Redox potential; NA: Not applicable; DL: Detection limit; NC: Not considered by the World Health organization.

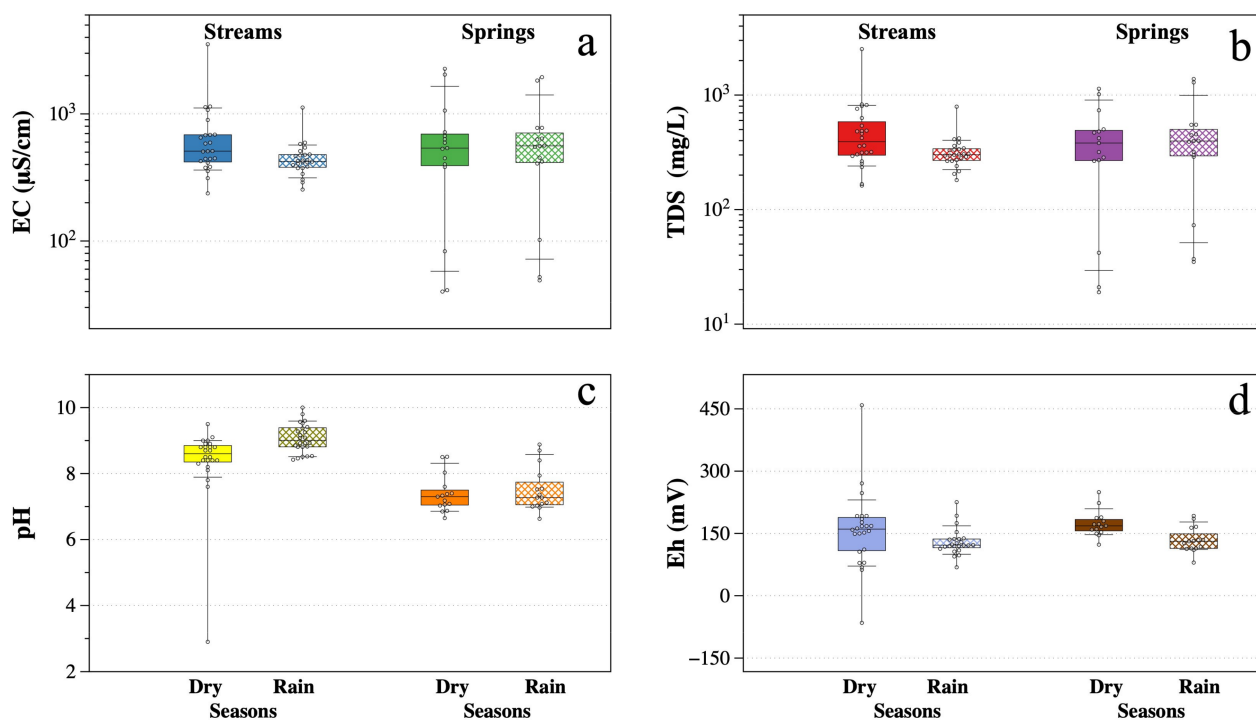


**Figure 2.** Box-and-Whisker plots for physicochemical parameters of surface water and springs for the dry and rainy seasons: (a) Electrical Conductivity (EC), (b) Total Dissolved Solids (TDS), (c) pH, and (d) oxidation–reduction potential (Eh).

### 3.2. Major and Minor Ions in Surface Water and Springs

Tables 1 and 2 show the major and minor ions in the surface water samples, for dry and rainy seasons, respectively. Table 3 shows the values recorded for ground water samples. The recorded concentrations of the  $\text{HCO}_3^-$  ion for surface water in the dry season had a median of 197.6, and of 201.3 mg/L in the rainy season (Figure 3a). For the springs, a median of 268.4 mg/L was recorded in the dry season and 261.1 mg/L in the rainy season (Figure 3b). The  $\text{SO}_4^{2-}$  content in the dry season for surface water had an observed median value of 61.5 and of 48.0 mg/L in the rainy season (Figure 3a). The maximum values of  $\text{SO}_4^{2-}$  content for both sampling periods were recorded in sample S2 (Table 1). For spring water, a median of 18.5 mg/L was reported for the dry season and of 15.0 mg/L for the rainy season (Figure 3b). The concentrations of  $\text{Cl}^-$  ions for surface water in the dry season was recorded at a median of 17.5 and of 10.0 mg/L in the rainy season (Figure 3a). For springs, the median was 5.4 mg/L in the dry season and 5.0 mg/L in the rainy season (Figure 3b). The concentrations of  $\text{NO}_3^-$  ions for surface water had a median of 7.1 mg/L during the dry season and of 1.4 mg/L in the rainy season (Figure 3a). For springs, the median was 1.4 mg/L in the dry season and 2.6 mg/L in the rainy season (Figure 3b). The concentrations of  $\text{Ca}^{2+}$  ions, for surface water in the dry season registered a median of 109.5 and of 97.7 mg/L in the rainy season (Figure 3a).

For springs, in the dry season the median was 112.2 and 83.9 mg/L in the rainy season (Figure 3b). The  $\text{Na}^{2+}$  ion concentration for surface water in the dry season had a median of 16.6 mg/L, whereas in the rainy season it was 9.3 mg/L (Figure 3a). For springs, the median was 5.3 mg/L in the dry season and 4.9 mg/L in the rainy season (Figure 3b). The  $\text{K}^+$  ion concentration for surface water in the dry season registered a median of 4.0 mg/L, and in the rainy season it was 2.2 mg/L (Figure 3a). For springs, the median was 0.9 mg/L in the dry season and 0.9 mg/L in the rainy season (Figure 3b). The  $\text{Mg}^{2+}$  ion concentrations for surface water had a median of 14.7 mg/L in the dry season and 10.2 mg/L in the rainy season (Figure 3a). For springs, the median was 4.2 mg/L in the dry season and 3.9 mg/L in the rainy season (Figure 3b). Finally, the concentration of  $\text{SiO}_2$  ions for surface water in the dry season registered a median of 14.7 and of 10.2 mg/L

in the rainy season (Figure 3a). For springs, the median value in the dry season was 4.2 and 3.9 mg/L in the rainy season (Figure 3b). Finally, a Piper’s diagram (Figure 4) shows the evolution of ground water represented by springs. The Na–Ca–HCO<sub>3</sub> facies originates in the recharge zone of the Sierra de Taxco in volcanic rocks of the Tilzapotla Rhyolite. The Ca–HCO<sub>3</sub> facie is in carbonate rocks of the Morelos and Mezcala formations and the Ca–SO<sub>4</sub> facie is located to the south of the sub-basin in the discharge zone of the water system (Figure 1). The statistical values of major and minor ions, measured in surface and ground water, from the Taxco-Cocula hydrological sub-basin are provided in Table S1 (Supplementary Material). The minimum (Min), maximum (Max), medians and the 10th percentile (P10), and 90th percentile (P90) values, as well as the interquartile range (IQR) show the behavior of major and minor ions and HM concentrations throughout the Taxco-Cocula hydrological sub-basin.

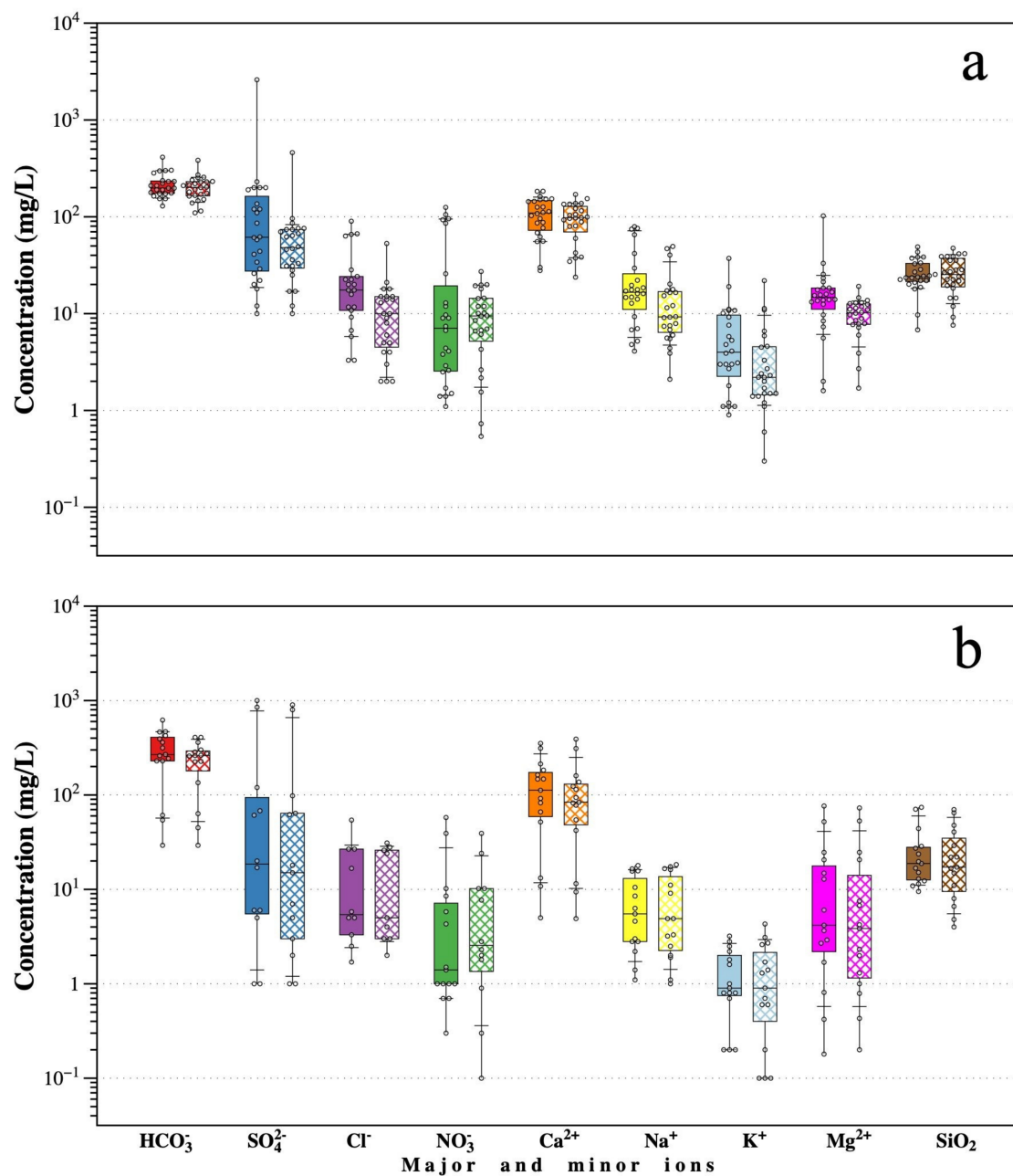


**Figure 3.** Box-and-Whisker plots for major and minor ions: (a) surface water and (b) springs for the dry (flat boxes) and rainy season (gridded boxes).

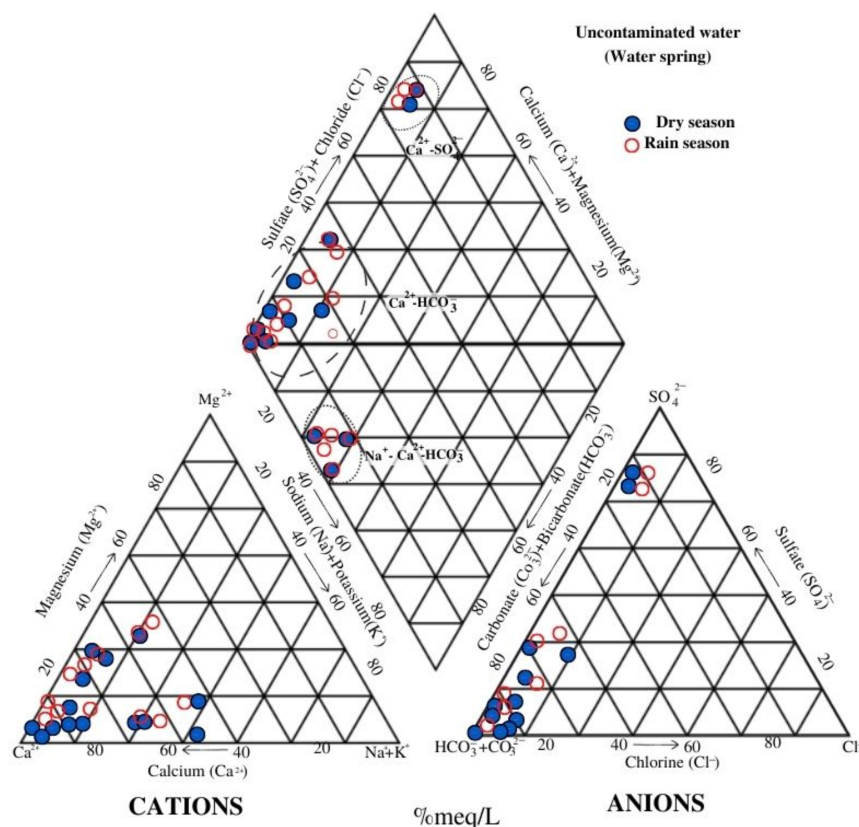


Figure 4. Piper diagram of the spring water for dry and rainy seasons.

### 3.3. Heavy Metals in Surface Water and Ground Water

Tables 4 and 5 show the HM concentrations of the surface water samples from dry and rainy seasons, respectively. Table 6 shows the HM concentrations recorded for ground water samples. Figure 1 of the HM distribution through the Taxco-Cocula hydrological sub-basin can be appreciated. Table S2 (Supplementary Material) shows the statistical values of the HM concentrations measured in surface and ground water from Taxco-Cocula hydrological sub-basin. In surface water in the dry season the aluminum (Al) concentration for the dry season ranged from 0.03 to 28.63 mg/L (Figure 5), with the maximum value recorded in sample S2 (Table 4). For the rainy season, Al concentration ranged from 0.05 to 2.15 mg/L, with the maximum value recorded in sample S8 (Table 5). According to Mexican regulation NOM-127-SSA1-2021 and the WHO standards for potable drinking water, the samples exceeding the permissible limit of 0.20 mg/L for Al were, for the dry season, S2, S3, S8, S10, S11, and S20, and, for the rainy season, S1–S4, S6, S8, S10, S13, S15, S16, and S19–S23 (Tables 4 and 5).

Table 4. Heavy metal concentrations in surface water samples: Dry season.

Sample	Al	As	Ba	Cd	Cu	Fe	Mn	Pb	Sr	Zn
	mg/L									
S1	0.05	0.01	0.03	0.01	<DL	0.16	0.40	<DL	0.16	0.45
S2	<b>28.63</b>	<b>0.60</b>	<b>0.03</b>	<b>1.78</b>	<b>1.05</b>	<b>68.27</b>	<b>21.47</b>	<b>0.02</b>	<b>0.45</b>	<b>208.80</b>
S3	1.65	0.02	0.03	0.10	0.08	3.10	1.58	<DL	0.19	13.28
S4	0.03	<DL	0.03	<DL	<DL	0.09	<DL	<DL	0.06	0.05
S5	<DL	<DL	0.02	<DL	<DL	0.06	<DL	<DL	0.08	0.08
S6	<DL	<DL	0.05	<DL	<DL	0.15	0.04	<DL	0.20	0.23
S7	0.06	<DL	0.06	<DL	<DL	0.14	<DL	<DL	0.37	0.23
S8	2.13	0.02	0.07	0.10	0.15	5.85	2.62	0.01	0.46	13.29

**Table 4.** *Cont.*

Sample	Al	As	Ba	Cd	Cu	Fe	Mn	Pb	Sr	Zn
	mg/L									
S9	<DL	<DL	0.05	<DL	<DL	0.06	<DL	<DL	0.29	0.07
S10	2.53	0.03	0.06	0.11	0.12	7.37	1.80	<DL	0.36	15.51
S11	0.27	0.01	0.05	0.07	<DL	1.03	1.58	<DL	0.29	7.36
S12	0.07	<DL	0.05	0.02	<DL	0.20	1.17	<DL	0.33	1.20
S13	0.03	<DL	0.04	<DL	<DL	0.04	<DL	<DL	0.20	0.11
S14	0.04	0.01	0.05	0.01	<DL	0.08	0.38	<DL	0.27	0.67
S15	0.03	<DL	0.05	<DL	<DL	0.05	<DL	<DL	0.22	0.08
S16	<DL	<DL	0.04	<DL	<DL	0.05	<DL	<DL	0.21	0.15
S17	<DL	<DL	0.07	<DL	<DL	0.04	<DL	<DL	0.41	0.05
S18	<DL	<DL	0.07	<DL	<DL	0.04	0.06	<DL	0.37	<DL
S19	0.03	0.01	0.08	<DL	<DL	0.23	0.67	<DL	0.30	0.15
S20	0.56	<DL	0.18	<DL	<DL	0.34	<DL	<DL	0.74	0.20
S21	0.06	<DL	0.17	<DL	<DL	0.06	<DL	<DL	0.73	<DL
S22	<DL	<DL	0.04	<DL	<DL	0.07	0.03	<DL	0.22	0.06
S23	0.05	<DL	0.04	<DL	<DL	0.04	0.03	<DL	0.21	0.10
S24	<DL	<DL	0.03	<DL	<DL	0.03	<DL	<DL	0.19	<DL
<b>Values established by the World Health Organization</b>										
	0.20	0.01	0.70	0.003	1.0	0.10	0.40	0.01	NC	5.0

DL: Detection limit; NC: Not considered by the World Health organization.

**Table 5.** Heavy metal concentrations in surface water samples: Rainy season.

Sample	Al	As	Ba	Cd	Cu	Fe	Mn	Pb	Sr	Zn
	mg/L									
S1	0.91	<DL	0.03	<DL	<DL	1.07	0.10	<DL	0.10	0.10
S2	0.25	<DL	<DL	0.02	<DL	0.94	0.59	<DL	0.45	1.41
S3	1.54	<DL	0.04	<DL	<DL	1.90	0.23	0.03	0.20	0.28
S4	0.13	<DL	0.03	<DL	<DL	0.15	<DL	<DL	0.09	<DL
S5	0.05	<DL	<DL	<DL	<DL	0.05	<DL	<DL	0.03	<DL
S6	0.13	<DL	0.05	<DL	<DL	0.19	0.05	<DL	0.20	0.12
S7	0.07	0.02	0.05	<DL	<DL	0.18	0.03	<DL	0.28	0.08
<b>S8</b>	<b>2.15</b>	<DL	0.05	<DL	<DL	3.73	0.25	0.05	0.19	0.42
S9	0.19	<DL	0.04	<DL	<DL	0.26	<DL	<DL	0.21	<DL
S10	0.23	0.01	0.04	0.01	<DL	0.36	0.06	<DL	0.29	0.09
S11	0.09	<DL	0.04	<DL	<DL	0.14	<DL	<DL	0.23	0.03
S12	0.12	<DL	0.03	<DL	<DL	0.17	<DL	<DL	0.18	0.03
S13	0.28	<DL	0.04	<DL	<DL	0.30	<DL	<DL	0.17	<DL
S14	0.12	<DL	0.03	<DL	<DL	0.18	<DL	<DL	0.30	<DL
S15	0.46	<DL	0.05	<DL	<DL	0.64	0.03	<DL	0.23	0.02
S16	0.34	0.09	0.04	<DL	<DL	0.51	0.03	<DL	0.22	0.05
S17	<DL	<DL	0.06	<DL	<DL	0.04	<DL	<DL	0.33	<DL
S18	<DL	0.02	0.06	<DL	<DL	0.04	<DL	<DL	0.37	0.03
S19	0.36	0.03	0.07	<DL	<DL	0.66	0.27	<DL	0.31	<DL
S20	0.88	<DL	0.22	<DL	<DL	0.54	0.03	<DL	0.92	0.03
S21	0.52	<DL	0.23	<DL	<DL	0.43	<DL	<DL	0.98	0.03
S22	0.52	0.01	0.05	<DL	<DL	0.65	0.04	<DL	0.26	0.05
S23	0.37	<DL	0.05	<DL	<DL	0.49	0.03	<DL	0.23	0.03
S24	0.11	<DL	0.04	<DL	<DL	0.12	<DL	<DL	0.17	<DL
<b>Values established by the World Health Organization</b>										
	0.20	0.01	0.70	0.003	1.0	0.10	0.40	0.01	NC	5.0

DL: Detection limit; NC: Not considered by the World Health organization.

**Table 6.** Heavy metal concentrations in ground water samples.

Sample	Al	As	Ba	Cd	Cu	Fe	Mn	Pb	Sr	Zn
	mg/L									
<b>Dry season</b>										
M1	0.37	<DL	0.07	<DL	<DL	0.13	<DL	<DL	0.03	0.14
M2	0.12	<DL	<DL	<DL	<DL	0.07	<DL	<DL	0.03	0.13
M3	0.03	<DL	<DL	<DL	<DL	<DL	<DL	<DL	<DL	0.05
M4	<DL	<DL	0.04	<DL	<DL	<DL	<DL	<DL	0.15	0.13
M5	<DL	<DL	0.04	<DL	<DL	0.10	0.03	<DL	0.20	0.07
M6	<DL	<DL	0.10	<DL	<DL	<DL	<DL	<DL	0.53	0.18
M7	<DL	<DL	0.05	<DL	<DL	<DL	<DL	<DL	0.31	0.09
M8	<DL	<DL	0.03	<DL	<DL	0.03	<DL	<DL	0.11	0.11
M9	0.03	0.012	<DL	<DL	<DL	<DL	<DL	<DL	0.07	<DL
M10	<DL	<DL	0.03	<DL	<DL	<DL	<DL	<DL	0.08	0.23
M11	0.15	<DL	<DL	<DL	<DL	0.05	<DL	<DL	0.05	0.04
M12	<DL	<DL	0.03	<DL	<DL	<DL	<DL	<DL	0.10	<DL
M13	<DL	<DL	<DL	<DL	<DL	0.05	<DL	<DL	2.55	0.09
M14	<DL	<DL	<DL	<DL	<DL	<DL	<DL	<DL	2.08	0.11
M15	<DL	0.081	0.04	<DL	<DL	<DL	<DL	<DL	1.00	0.03
<b>Rainy Season</b>										
M1	0.05	<DL	0.05	<DL	<DL	0.03	<DL	<DL	0.05	0.06
M2	0.21	<DL	<DL	<DL	<DL	0.25	<DL	<DL	0.03	<DL
M3	<DL	<DL	<DL	<DL	<DL	<DL	<DL	<DL	0.03	<DL
M4	0.03	<DL	0.04	<DL	<DL	0.05	<DL	<DL	0.13	<DL
M5	<DL	<DL	0.04	<DL	<DL	0.14	0.03	<DL	0.18	<DL
M6	0.10	<DL	0.05	<DL	<DL	0.14	<DL	<DL	0.33	<DL
M7	<DL	<DL	0.06	<DL	<DL	<DL	<DL	<DL	0.03	<DL
M8	<DL	<DL	<DL	<DL	<DL	<DL	<DL	<DL	0.07	<DL
M9	0.17	<DL	<DL	<DL	<DL	0.04	<DL	<DL	0.04	<DL
M10	0.07	<DL	<DL	<DL	<DL	0.06	<DL	<DL	0.05	<DL
M11	0.25	<DL	0.03	<DL	<DL	0.13	<DL	<DL	0.06	<DL
M12	<DL	<DL	<DL	<DL	<DL	0.02	<DL	<DL	0.04	<DL
M13	<DL	<DL	<DL	<DL	<DL	0.06	<DL	<DL	2.80	0.03
M14	<DL	<DL	<DL	<DL	<DL	<DL	<DL	<DL	1.90	<DL
M15	<DL	0.15	0.07	<DL	<DL	0.10	<DL	<DL	1.88	<DL
<b>Values established by the World Health Organization</b>										
	0.20	0.01	0.70	0.003	1.0	0.10	0.40	0.01	NC	5.0

DL: Detection limit; NC: Not considered by the World Health organization.

With respect to the arsenic (As) in surface water, in the dry season, the concentration ranged from 0.01 to 0.60 mg/L (Figure 5a), with the maximum concentration in sample S2 (Table 4). In the rainy season, concentrations ranged from 0.01 to 0.09 mg/L, with the maximum value in sample S16. According to Mexican regulations, the samples that exceeded the permissible limit of 0.05 mg/L for As were S2 in the dry season and S16 in the rainy season. Additionally, according to the WHO [16], the samples that exceeded the permissible limit of 0.01 mg/L were S2, S3, S8, S10 for the dry season and S7, S16, S17, and S19 for the rainy season (Tables 4 and 5).

Cadmium (Cd) was detected in surface water in the dry season, with concentrations ranging from 0.01 to 1.78 mg/L, with the maximum value recorded in sample S2. For the rainy season, values of 0.02 and 0.01 mg/L were recorded. All samples in both sampling seasons exceeded the permissible limits of 0.005 and 0.003 mg/L, respectively, established by Mexican regulations and the WHO [15,16] for this element (Tables 4 and 5).

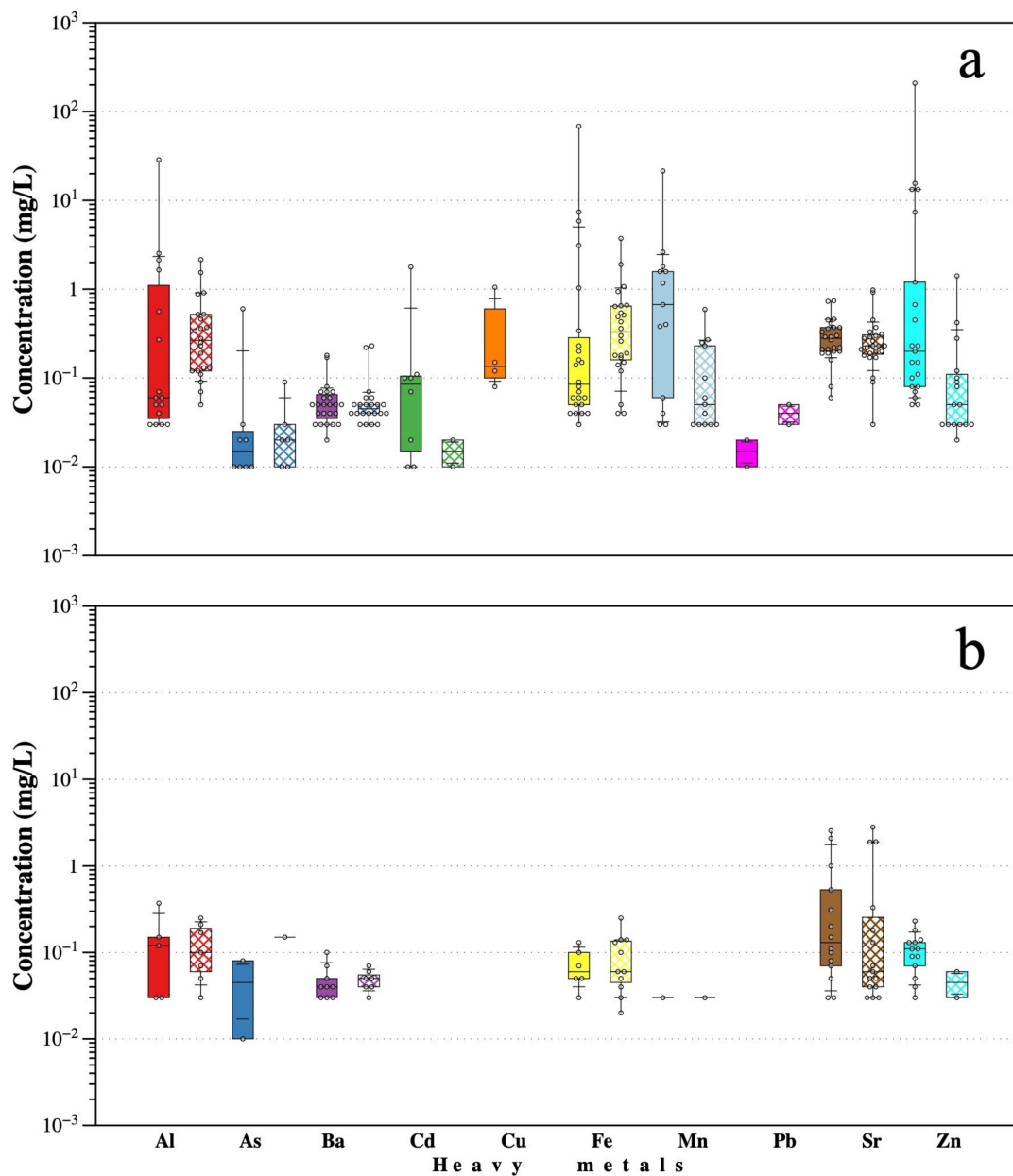


**Figure 5.** Box-and-Whisker plots of the heavy metal concentrations in dry season (flat boxes) and rainy season (gridded boxes) in (a) surface water and (b) springs.

Copper (Cu) was detected in the dry season (surface water), with values ranging from 0.12 to 1.05 mg/L, with the maximum value in sample S2, which exceeded the WHO limit of 1.0 mg/L (Table 4). No concentrations of this element were recorded during the rainy season (Table 5).

In surface water in the dry season, the iron (Fe) values ranged from 0.03 to 68.27 mg/L (Figure 5, Table 4), with the maximum value measured in sample S2. In the rainy season, values generally decreased and ranged from 0.04 to 3.73 mg/L, with the maximum value in sample S8. According to the Mexican standard, samples exceeding the permissible limit of 0.300 mg/L for Fe were S2, S3, S8, S10, S11, and S20 for the dry season, and, for the rainy season, S1–S3, S8, S10, S15, S16, and S19–S23. According to the WHO, the samples that exceeded the permissible limit of 0.10 mg/L were S1–S3, S6–S8, S10–S12, S19 and S20 for the dry season, while, for the rainy season, almost all samples exceeded the limit, except for S5, S16, and S18 (Figure 6, Tables 4 and 5).

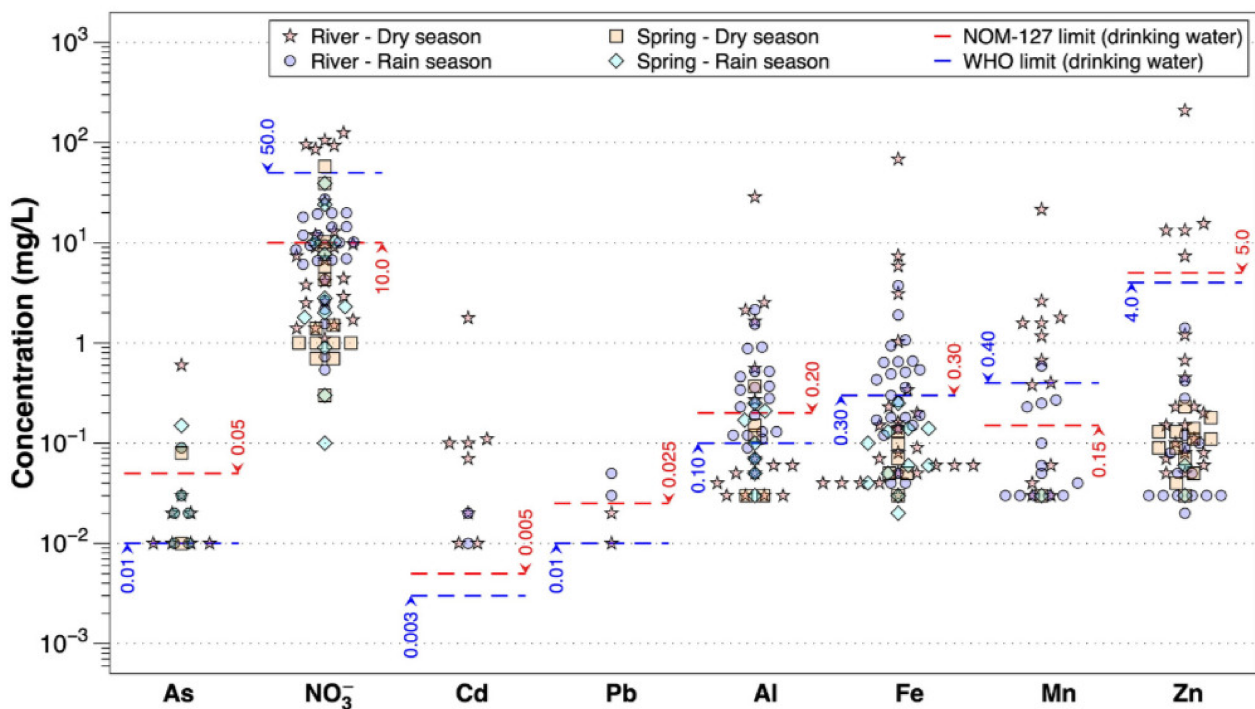


**Figure 6.** Heavy metal and nitrate concentrations at each sampling site for surface water and springs, and international standards for water for human consumption [15,16].

In the case of manganese (Mn) in surface water in the dry season values ranged from 0.02 to 21.47 mg/L, with the maximum value present in sample S2. For the rainy season, concentrations ranged from 0.03 to 0.59 mg/L, with the maximum value in sample S2. According to Mexican regulations, samples exceeding the permissible limit of 0.025 mg/L for Mn were S1–S3, S8, S10–S12, S14, and S17 for the dry season, while for the rainy season they were S2, S3, S8 and S19. Additionally, according to the WHO, the samples that exceeded the 0.40 mg/L limit for Mn were the same samples as those that flouted the Mexican standard, except for S1 and S14 for the dry season, and, for the rainy season, only S2 exceeded the WHO standard (Figure 6, Tables 4 and 5).

With respect to the presence of lead (Pb), it was detected in surface water in the dry season in samples S2 and S8, with concentrations of 0.02 and 0.01 mg/L, respectively, and, in the rainy season, Pb was detected in samples S3 and S8, with concentrations of 0.03 and 0.05 mg/L, which exceeded the limits of 0.025 mg/L and 0.01 mg/L established by Mexican regulations and the WHO, respectively (Figure 6, Tables 4 and 5). Zinc (Zn) was the metal with the highest concentrations in surface runoffs, observed in most of the samples. For instance, in the dry season, the values for Zn ranged from 0.05 to 208.80 mg/L (Figure 5a), except for samples S18, S21 and S24, which presented concentrations < DL. The maximum value was recorded in sample S2. For the rainy season, a decrease in concentrations were observed, with values ranging from 0.02 to 1.41 mg/L, while the maximum value coincided with sample S2. According to Mexican and WHO regulations, the samples that exceeded the permissible limit of 5.0 mg/L were S2, S3, S8, S10, and S12, in the dry season (Figure 6, Tables 4 and 5).

Although barium (Ba) and strontium (Sr) are not addressed in NOM-127 or by the WHO, they were considered in this study due to their constant presence in high concentrations in the sampled water. In the case of Ba concentration, in the dry season all samples had values that ranged from 0.02 to 0.18 mg/L (Figure 5a), with the maximum value recorded in sample S20. For the rainy season, concentrations ranged from 0.03 to 0.23 mg/L, except for samples S2 and S5, which were < DL (Tables 4 and 5). Strontium (Sr) was detected in all samples, ranging from 0.06 to 0.74 mg/L in the dry season (Figure 5a), with the maximum value recorded in sample S20. For the rainy season, the concentration ranged from 0.03

to 0.98 mg/L, with the maximum values present in samples S21 and S20 (Tables 4 and 5). The HM concentrations observed in spring waters are shown in Table 6. During the dry season, Al concentrations in samples M1–M3, M9, and M11 ranged from 0.03 to 0.37 mg/L (Figure 5b) and in the rainy season it was detected in M1, M2, M4, M6, M9, M10, and M11 with concentrations from 0.03 to 0.25 mg/L (Figures 1 and 5b, Table 6).

In the dry season, samples M9 and M15 reported arsenic concentrations of 0.01 and 0.08 mg/L, respectively, while in the rainy season arsenic was measured only in M15, with a concentration of 0.15 mg/L. The spring concerned is located south of the area, in the discharge zone of the Taxco-Cocula sub-basin (Figures 1 and 5b, Table 6).

Ba for the dry season was detected in springs M1, M4–M8, M10, M12, and M15, with concentrations of 0.03 to 0.10 mg/L (Figure 5b). For the rainy season, Ba was detected in the same springs, except for M8 and M12, with concentrations of 0.03 to 0.07 mg/L. This element was measured in springs located in the recharge and discharge zones (Figures 1 and 5b, Table 6).

Fe concentrations for the dry season in springs M1, M2, M5, M8, M11, and M13 ranged from 0.03 to 0.13 mg/L (Figure 5b), while for the rainy season, Fe was measured in 11 springs with concentrations from 0.02 to 0.25 mg/L. For springs M1 and M2 (located in the recharge zone) concentrations of 0.03 and 0.25 mg/L (maximum value), respectively, were measured. For the discharge zone, Fe concentrations in springs M13 and M15 were 0.06 and 0.10 mg/L, respectively (Figures 1 and 5b, Table 6). This behavior indicates that the release of Fe compounds into the ground water occurs mainly in the rainy season. Regarding Mn, it was found only in sample M5 in both sampling seasons, with a concentration of 0.03 mg/L (Figure 5b, Table 6).

Sr concentration for the dry season was measured in 14 springs, ranging from 0.03 to 2.55 mg/L, except in M3, where the value was < DL. For the rainy season, the Sr concentration ranged from 0.03 to 2.80 mg/L. In springs M1–M3 (located in the recharge zone), for both sampling seasons, the Sr concentrations were consistently low, in the order of 0.03 mg/L, contrary to those of the discharge zone M13–M15, where the maximum values were found (Figures 1 and 5b, Table 6).

The Zn concentration for the dry season ranged from 0.03 to 0.23 mg/L (Figure 5), except for springs M9 and M12, where the concentrations were < DL. In the rainy season, Zn was only detected in springs M1 and M13, with concentrations of 0.06 and 0.03 mg/L, respectively. This behavior indicates that the release of Zn into ground water occurs preferentially during the dry season, behavior opposite to that of Fe (Figures 1 and 5b, Table 6).

Cd, Cu, and Pb for spring water were found to be < DL (in both seasons) (Figure 5b, Table 6). In regard to the hydrogeochemical characteristics of springs, we considered those with low HM concentrations to be the sum of natural chemical reactions with ground water and minerals contained in the rocks without influence from mining activities.

## 4. Discussion

### 4.1. The Origin of Contaminants in Surface Water

The correlations found between dissolved species reveals that the origin of solutes and the main processes are related to the evolution of the surface water. In Table 7, a correlation coefficient matrix ( $p$ -value < 0.05) for surface water in the dry season is presented, coinciding with the season with higher HM concentrations. A highly positive correlation ( $r = 0.97$ ) was observed between EC and TDS. The observed correlation between EC and TDS with major ions  $\text{SO}_4^{2-}$  and  $\text{Mg}^{2+}$  was high ( $r > 0.92$ ), as well as with Al, As, Cd, Cu, Fe, Mn, Pb, and Zn ( $r > 0.89$ ) and with  $\text{NO}_3^-$  ion ( $r > 0.76$ ). It is considered that pH has an important role in HM release, having a highly negative correlation with Al, As, Cd, Cu, Fe, Mn, Pb, and Zn ( $r > -0.87$ ), and even higher with  $\text{SO}_4^{2-}$  ions ( $r = -0.95$ ). On the contrary, for the Eh values, the correlations were moderately positive with major ions  $\text{SO}_4^{2-}$  and  $\text{Mg}^{2+}$  ( $r > 0.69$ ), as well as with Al, As, Cd, Cu, Fe, Mn, Pb, and Zn ( $r = 0.67$ – $0.70$ ). The  $\text{SO}_4^{2-}$  ion showed high positive correlations with Al, As, Cd, Cu, Fe, Mn, Pb, and Zn ( $r > 0.91$ ).

**Table 7.** Correlation coefficient matrix (*p*-value < 0.05) for chemical composition of surface water in dry season.

	EC	TDS	pH	Eh	HCO <sub>3</sub> <sup>-</sup>	SO <sub>4</sub> <sup>2-</sup>	Cl <sup>-</sup>	NO <sub>3</sub> <sup>-</sup>	Ca <sup>2+</sup>	Na <sup>+</sup>	K <sup>+</sup>	Mg <sup>2+</sup>	SiO <sub>2</sub>	Al	As	Ba	Cd	Cu	Fe	Mn	Pb	Sr	Zn	
EC	1.00																							
TDS	0.97	1.00																						
pH	-0.94	-0.92	1.00																					
Eh	0.59	0.62	-0.60	1.00																				
HCO <sub>3</sub> <sup>-</sup>	-0.32	-0.35	0.40	-0.52	1.00																			
SO <sub>4</sub> <sup>2-</sup>	0.95	0.94	-0.94	0.69	-0.56	1.00																		
Cl <sup>-</sup>	0.14	0.14	0.00	-0.25	0.66	-0.14	1.00																	
NO <sub>3</sub> <sup>-</sup>	0.77	0.76	-0.64	0.26	0.14	0.57	0.68	1.00																
Ca <sup>2+</sup>	0.30	0.37	-0.23	0.45	-0.04	0.27	0.06	0.09	1.00															
Na <sup>+</sup>	0.30	0.31	-0.17	-0.21	0.52	0.04	0.92	0.79	-0.04	1.00														
K <sup>+</sup>	0.11	0.11	-0.02	-0.10	0.38	-0.11	0.83	0.52	0.02	0.77	1.00													
Mg <sup>2+</sup>	0.92	0.94	-0.89	0.70	-0.54	0.95	-0.06	0.56	0.47	0.08	0.02	1.00												
SiO <sub>2</sub>	0.03	0.08	0.02	0.21	0.30	-0.12	0.53	0.30	0.47	0.36	0.51	-0.02	1.00											
Al	0.94	0.93	-0.95	0.68	-0.58	0.99	-0.15	0.57	0.24	0.03	-0.10	0.95	-0.12	1.00										
As	0.94	0.92	-0.94	0.69	-0.56	0.99	-0.16	0.56	0.22	0.01	-0.11	0.94	-0.14	1.00	1.00									
Ba	-0.18	-0.17	0.15	-0.23	-0.03	-0.17	-0.01	-0.21	-0.10	0.11	0.35	-0.07	-0.27	-0.16	-0.18	1.00								
Cd	0.94	0.93	-0.95	0.69	-0.58	0.99	-0.16	0.56	0.24	0.02	-0.11	0.95	-0.13	0.99	0.99	-0.18	1.00							
Cu	0.95	0.94	-0.94	0.68	-0.57	0.99	-0.11	0.60	0.27	0.06	-0.08	0.95	-0.08	0.99	0.99	-0.17	0.99	1.00						
Fe	0.94	0.94	-0.94	0.70	-0.58	0.99	-0.15	0.57	0.25	0.03	-0.10	0.95	-0.11	0.99	0.99	-0.17	1.00	0.99	1.00					
Mn	0.95	0.95	-0.94	0.70	-0.57	0.99	-0.11	0.60	0.28	0.07	-0.06	0.96	-0.08	0.99	0.99	-0.18	1.00	0.99	0.99	1.00				
Pb	0.91	0.89	-0.87	0.67	-0.55	0.92	-0.03	0.62	0.34	0.13	0.02	0.93	0.00	0.93	0.91	-0.14	0.92	0.95	0.93	0.94	1.00			
Sr	0.20	0.22	-0.20	0.07	-0.18	0.20	-0.02	0.02	0.25	0.14	0.30	0.35	-0.20	0.20	0.18	0.89	0.19	0.20	0.20	0.20	0.25	1.00		
Zn	0.94	0.93	-0.95	0.69	-0.57	0.99	-0.15	0.57	0.24	0.03	-0.11	0.95	-0.12	0.99	0.99	-0.18	0.99	0.99	0.99	0.99	0.92	0.19	1.00	

EC: Electrical conductivity; TDS: Total dissolved solids; Eh: Redox potential. The cells highlighted have coefficients higher than 0.7.

Although the main surface runoff of the study area comprises a total of 80 km, previous studies have focused on the northern part of the hydrological sub-basin. Those studies evaluated pollution from the mining along only 8 km of the Cacalotenango and Taxco Rivers [3,12,13,33]. However, the interaction of meteoric water with mining tailings produced AMD with high concentrations of As, Pb, Cd, Cu, Fe, Mn, and Zn with  $\text{pH} < 3$  [10,28,34]. The AMD is continuously incorporated into the surface drainage near the mining complexes. For instance, sample S2 stood out as a generating point for AMD [35,36]. This sampling site is in the northern part of the hydrological recharge zone of the Taxco-Cocula sub-basin. The correlations highlight the common origin of the  $\text{SO}_4^{2-}$  anion and the HMs in the northern portion of the sub-basin.

On the other hand, the exclusively high positive correlation between Ba and Sr ( $r = 0.89$ ) may be related to water–rock interaction [6]. Lack of correlations between  $\text{NO}_3^-$  ions and HMs and major ions were found, except for  $\text{Na}^+$  ( $r = 0.79$ ), which might be related to the mixing of surface water and urban wastewater [37] (Table 7).

The correlation coefficient matrix obtained for the rainy season is shown in Table 8. Moderate and high positive correlations among EC and TDS with major ions  $\text{SO}_4^{2-}$  and  $\text{Mg}^{2+}$  ( $r = 0.91$  and  $0.70$ ) and Cd, Mn, and Zn ( $r > 0.75$ ), and low moderate correlations with Eh and  $\text{NO}_3^-$  ( $r = 0.53$  and  $0.52$ ), were observed. Furthermore,  $\text{SO}_4^{2-}$  ions presented a moderate positive correlation with  $\text{Mg}^{2+}$  ( $r = 0.57$ ) and high correlations with Zn ( $r = 0.95$ ), Mn ( $r = 0.83$ ), and Cd ( $r = 0.92$ ). Lower correlations ( $r < 0.54$ ) between  $\text{SO}_4^{2-}$  and the HMs evidenced dilution processes that occur each rainy season. However, high positive correlations between  $\text{SO}_4^{2-}$ , Cd, Mn, and Zn ( $r > 0.83$ ), Al and Mn ( $r = 0.88$ ), Cd, Fe, and Zn ( $r > 0.75$ ), Fe and Mn ( $r = 0.90$ ), and Mn and Zn ( $r = 0.90$ ) were consistent with the common origin of the HMs coming from mining tailings carried by surface water. In the rainy season high positive correlations between Ba and Sr ( $r = 0.91$ ) were also observed. Romero et al. [28] and Talavera Mendoza et al. [3,9,10] showed that tailings exposed to natural runoff from main water tributaries, such as the Taxco River and the Cacalotenango River, had high contents of HMs, due to the oxidation of sulfurous minerals, mainly pyrite. Isotopic studies confirmed that sulfates in the area influence the mineralization of tailings, as well as of Pb and Sr [3], and that the dry season is marked by evaporation processes and rainfall by dilution that influence the decrease HM concentrations in the area [3,12].

Recently, Quevedo-Castañón et al. [35] suggested that natural mixing of AMD with natural runoff water from streams in the area helped with AMD neutralization in Taxco. This is consistent with the correlation analysis of the rainy season that evidenced this component. A multivariate analysis was performed to improve the contrast between physicochemical variables, major ions, and the HMs in the dry season, by using Principal Component Analysis. Table S3 (Supplementary Material) shows the concentration values and the percentages of total variance for each variable. Component 1 explained 55.0% of the variance, related to  $\text{SO}_4^{2-}$ ,  $\text{Mg}^{2+}$ ,  $\text{Cu}^{2+}$ ,  $\text{Mn}^{4+}$ ,  $\text{Al}^{3+}$ ,  $\text{As}^{5+}$ ,  $\text{Cd}^{2+}$ ,  $\text{Pb}^{2+}$ , and  $\text{Zn}^{2+}$ , confirming their origins as being from mining tailings. Component 2 explained 20.5% of the variance and the higher weight was associated with  $\text{HCO}_3^-$ ,  $\text{Cl}^-$ ,  $\text{NO}_3^-$ ,  $\text{Na}^+$ ,  $\text{SiO}_2$ , and  $\text{K}^+$  variables, suggesting mixing with rainwater and urban wastewater. Component 3 explained 11.2% of the variance, with the higher weight associated with  $\text{Ba}^{2+}$ ,  $\text{Sr}^{2+}$ , and  $\text{Ca}^{2+}$ , as suggested in the correlation analysis. Figure 7 presents the three main components associated with the multivariate analysis, confirming the processes associated with the observed chemistry on surface water, which were also in accordance with the correlation matrices for both the rainy and dry seasons.

**Table 8.** Correlation coefficient matrix ( $p$ -value < 0.05) for chemical composition of surface water in rainy season.

	EC	TDS	pH	Eh	HCO <sub>3</sub> <sup>-</sup>	SO <sub>4</sub> <sup>2-</sup>	Cl <sup>-</sup>	NO <sub>3</sub> <sup>-</sup>	Ca <sup>2+</sup>	Na <sup>+</sup>	K <sup>+</sup>	Mg <sup>2+</sup>	SiO <sub>2</sub>	Al	As	Ba	Cd	Fe	Mn	Pb	Sr	Zn	
EC	1.00																						
TDS	<b>1.00</b>	1.00																					
pH	-0.28	-0.28	1.00																				
Eh	0.53	0.53	-0.47	1.00																			
HCO <sub>3</sub> <sup>-</sup>	0.29	0.29	0.09	0.08	1.00																		
SO <sub>4</sub> <sup>2-</sup>	<b>0.91</b>	<b>0.91</b>	-0.25	0.59	0.13	1.00																	
Cl <sup>-</sup>	0.47	0.47	-0.28	0.08	-0.01	0.27	1.00																
NO <sub>3</sub> <sup>-</sup>	0.52	0.52	<b>-0.74</b>	0.32	-0.01	0.38	<b>0.72</b>	1.00															
Ca <sup>2+</sup>	0.47	0.47	-0.41	0.31	0.53	0.27	-0.10	0.20	1.00														
Na <sup>+</sup>	0.26	0.25	0.26	-0.18	-0.22	0.23	0.65	0.13	-0.41	1.00													
K <sup>+</sup>	0.14	0.14	-0.02	-0.18	-0.23	0.02	<b>0.84</b>	0.38	-0.35	<b>0.85</b>	1.00												
Mg <sup>2+</sup>	<b>0.70</b>	<b>0.71</b>	-0.21	0.14	0.34	0.57	0.38	0.33	0.59	0.40	0.32	1.00											
SiO <sub>2</sub>	0.01	0.01	-0.39	-0.01	0.01	-0.14	0.23	0.44	0.37	-0.18	0.14	0.14	1.00										
Al	-0.10	-0.10	-0.40	0.08	-0.46	0.07	0.08	0.25	-0.14	0.23	0.23	0.13	0.23	1.00									
As	0.01	0.02	-0.16	-0.07	0.02	-0.11	0.11	0.07	0.21	-0.01	0.12	0.21	0.16	-0.10	1.00								
Ba	-0.13	-0.13	0.51	-0.41	-0.16	-0.12	0.18	-0.34	-0.36	<b>0.81</b>	0.57	0.29	-0.30	0.18	-0.04	1.00							
Cd	<b>0.87</b>	0.87	-0.22	0.60	0.26	<b>0.92</b>	0.21	0.33	0.38	0.09	-0.08	0.53	-0.15	-0.09	-0.06	-0.22	1.00						
Fe	0.07	0.07	-0.54	0.21	-0.36	0.20	0.12	0.36	0.02	0.09	0.15	0.18	0.32	<b>0.94</b>	-0.06	-0.03	0.07	1.00					
Mn	<b>0.75</b>	<b>0.75</b>	-0.57	0.61	-0.08	<b>0.83</b>	0.49	0.63	0.20	0.25	0.28	0.50	0.15	0.39	-0.02	-0.20	<b>0.75</b>	0.54	1.00				
Pb	-0.07	-0.07	-0.43	0.08	-0.32	0.06	0.01	0.26	0.01	-0.01	0.08	0.08	0.45	<b>0.88</b>	-0.11	-0.06	-0.08	<b>0.93</b>	0.37	1.00			
Sr	0.26	0.26	0.45	-0.21	-0.02	0.25	0.27	-0.21	-0.17	<b>0.84</b>	0.54	0.54	-0.37	0.09	-0.04	<b>0.91</b>	0.14	-0.05	0.06	-0.13	1.00		
Zn	<b>0.82</b>	<b>0.82</b>	-0.39	<b>0.65</b>	0.07	<b>0.95</b>	0.18	0.37	0.31	0.08	-0.05	0.51	-0.04	0.23	-0.10	-0.23	<b>0.88</b>	0.40	<b>0.90</b>	0.25	0.10	1.00	

EC: Electrical conductivity; TDS: Total dissolved solids; Eh: Redox potential. The cells highlighted have coefficients higher than 0.7.

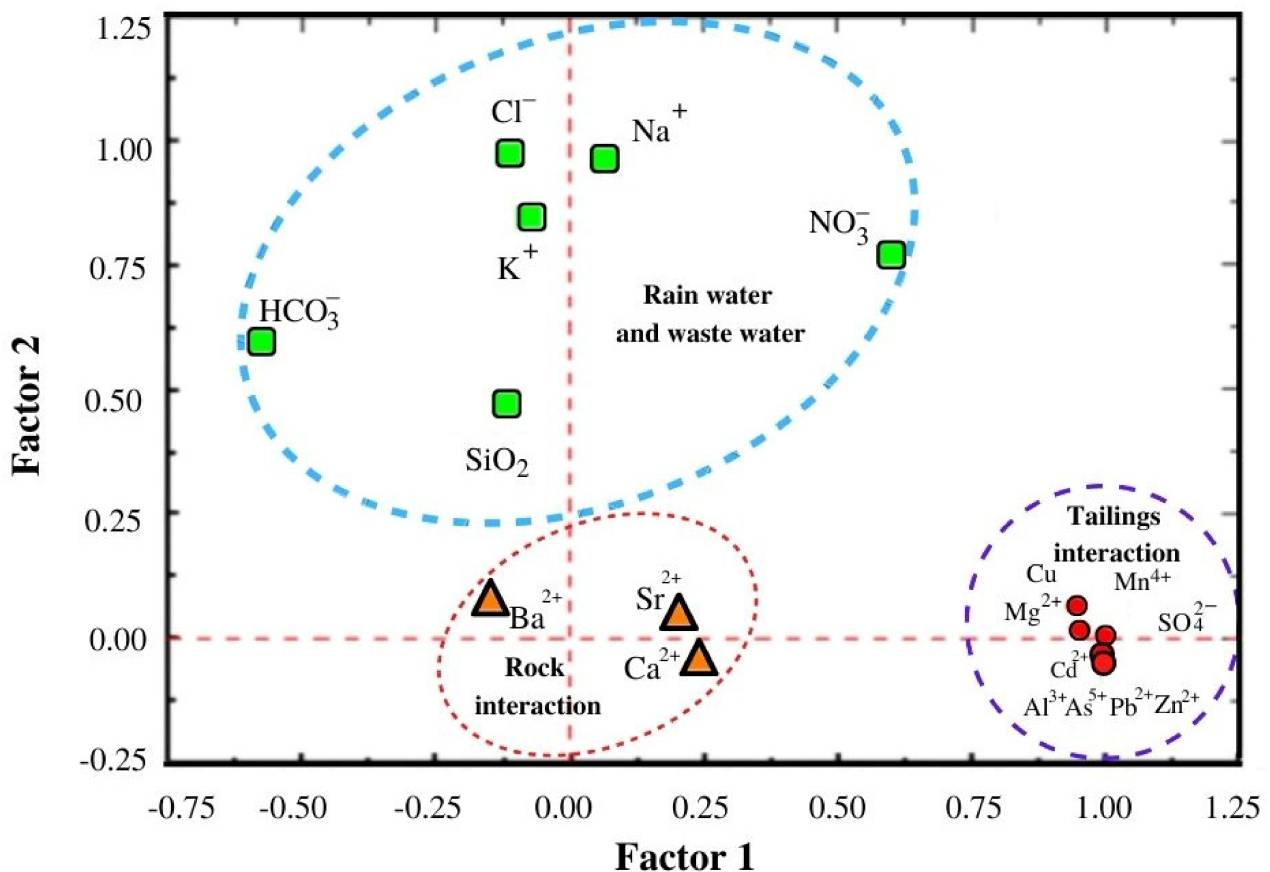


**Figure 7.** Principal components analysis for surface water samples for the dry season.

#### 4.2. Contaminant Dispersion Mechanisms on the Taxco-Cocula Sub-Basin

Findings from this research, as well as from research conducted by Armienta et al. [33,34], Talavera Mendoza et al. [9,10], and Romero et al. [28], agree that the main influence of the mining is in the north of the TMD. The dispersion of HMs in the sub-basin begins with the rainwater that infiltrates the tailings, leaching and entraining particles. The hydration of this material is the first step in the incorporation of HMs in the nearby rivers and streams, by the weathering of minerals, such as anhydrite to gypsum [38]. The different tailing deposits are in a surface area of ~25 km<sup>2</sup>. Although they have the same origins and are separated from each other, there are differences in their geochemical and environmental behaviors, as evidenced by the HM concentrations.

Acid generating minerals were identified by Bancks et al. [39] and Dold [40] in the MS<sub>2</sub> form, as pyrite (FeS<sub>2</sub>) and pyrrhotite (Fe<sub>1-x</sub>S<sub>2</sub>), and non-acid generating minerals can be generalized in the MS form, as galena (PbS), chalcopyrite (CuFeS<sub>2</sub>), sphalerite (ZnS), and arsenopyrite (AsFeS), among others. In this generalization, M<sup>+</sup> represents the divalent cation. For instance, Taxco ore deposit was previously characterized. Minerals, such as Pyrite (10–15%), sphalerite (11%), galena (4%), and other secondary minerals, such as chalcopyrite, argentite, pyrrargyrite, pyrolusite, and arsenopyrite, were identified by Talavera Mendoza et al. [9] and Romero et al. [28].

Sampling site S2 was close to the Guerrero II tailings, where the last processing plant operated, and the lowest pH value was recorded there (Table 1, Figure 1). Thus, the channel that drains the leachates concentrates the oxidation processes of primary, secondary, and gangue minerals that lead to the generation of AMD, evidenced by the physicochemical characteristics and higher concentrations of HMs in the surface water of the entire sub-basin. In 2016, IMMSA (the company in charge of mining liabilities), intensified remediation activities, by reducing slopes in tailing dams, compacting slopes with calcareous gravel, constructing filters to reduce the pollutant discharges from tailings to the main tributaries,

and eliminating mine water in rivers and streams, as well as phytoremediation in the zone. The impact of these remediation processes on the tailings could be quantified with new analyses to assess the variations associated with sites with high concentrations of HMs in the Taxco-Cocula sub-basin.

By contrast, the measurements of the same parameters in springs in the dry and rainy seasons did not present significant changes and were related to peripheral water, evidenced by the high concentrations of  $\text{HCO}_3^-$ . The differences between the chemical facies are due to the geology in which the springs are located as their hydrogeochemical characteristics in the dry and rainy seasons do not vary significantly, in congruence with the physical-chemical parameters measured in situ. The geology of the zone plays a key role in diminishing the hazardous effects of AMD [36,41] (Table 3, Figure 1).

According to previous results, one can conclude that the highest concentrations of the analyzed HMs (Al, As, Ba, Cd, Cu, Fe, Mn, Pb, Sr, and Zn) are mainly found in the Cacalotenango River, having concentrations in the range of the values reported by Talavera Mendoza et al. [9]. Moreover, in Taxco River, Quevedo-Castañón et al. [35], reported on the behavior involved in the generation of AMD in a small tributary of the Taxco River, with extreme values of  $\text{pH} < 3.0$  and high concentrations of HMs measured in total concentration and in soluble elements. They also reported data on Pb isotopes, which showed chemical signatures similar to the mineral deposits of Taxco, as well as the reactive mineral phases that control AMD. The results of this work showed that in both the Taxco and Cacalotenango Rivers, metal leaching was magnified during the rainy season.

#### 4.3. Speciation and Saturation Index (SI)

Tables S4 and S5 (Supplementary Material) show the behaviors at each sampled point for the dry and rainy seasons, respectively. The spatial and temporal chemical variations of the surface water of the Taxco-Cocula sub-basin were consistent with the diversity of reactive phases, which control the concentration and distribution of HMs downstream of the main source of pollutant emissions (S2).

An SI value of zero, with an associated uncertainty ( $\pm 0.1$ ), indicates that mineral precipitation (supersaturation) is possible, while a value less than zero indicates that mineral dissolution (sub-saturation) is possible. These calculations assume that the dissolved species in surface water are in chemical equilibrium [42].

The main saturated phases were aragonite, calcite ( $\text{CaCO}_3$ ), goethite ( $\text{FeOOH}$ ), quartz ( $\text{SiO}_2$ ), barite ( $\text{BaSO}_4$ ) and zincite ( $\text{ZnO}$ ), which appear to control the concentration and partition of the HMs in all areas of the sub-basin. The aragonite and calcite in all samples were saturated, except in sample S2, where AMD was reported.

Jarosite [ $(\text{K}, \text{Na}, \text{H})\text{Fe}_3(\text{SO}_4)_2(\text{OH})_6$ ] and goethite ( $\text{FeOOH}$ ) were subsaturated in sample S2. However, at sites S3, S8 and S10 the saturation indices were  $>0$  for jarosite, so this phase could precipitate at these sites, which are close to S2 (Figure 1). All samples after S11 through to S24 were unsaturated in Jarosite, indicating the aqueous phase. Goethite was saturated in all other samples, even in the rainy season.

Talavera Mendoza et al. [9] and Romero et al. [43] identified fluorescent minerals and gypsum as evidence of proton neutralization by calcite. These fluorescent minerals were observed in the dry season at points S2, S3, and S4 and were identified near the sampling sites. For the Taxco-Cocula River segment at site S2, cuprousferrite ( $\text{CuFeO}_2$ ) was supersaturated, while Anglesite ( $\text{PbSO}_4$ ), tenorite ( $\text{CuO}$ ), and compounds of  $\text{As}_2\text{O}_3$ , and  $\text{CdSO}_4$  were subsaturated. These behaviors were related to  $\text{pH} = 2.9$  and  $\text{Eh} = 458.7$  mV. The S3 site near the AMD generation site was the only site where reducing potential was recorded ( $-65.4$  mV), and here the compounds were saturated, Otavita ( $\text{CdCO}_3$ ) Tenorite ( $\text{CuO}$ ),  $\text{AlOOH}$ , and  $\text{Ba}_3(\text{AsO}_4)_2$ .

After sample S8 the compounds changed, highlighting the carbonates of cadmium, manganese, and magnesium, in addition to  $\text{Ba}_3(\text{AsO}_4)_2$ , and  $\text{AlOOH}$ , that occurred mainly up to sample S14. From samples S16 to S23, the presence of willemite ( $\text{Zn}_2\text{SiO}_4$ ) was present

in a saturated form, while the  $\text{MgCO}_3$  saturation index was near equilibrium, and siderite ( $\text{FeCO}_3$ ) and  $\text{SrSO}_4$  were unsaturated.

For the Cacalotenango stream segment, in samples S4, S5, S6, and S7, the change in compounds, where willemite was saturated, stood out, as well as  $\text{AlOOH}$  and  $\text{Al}(\text{OH})_3$ , while siderite and  $\text{MgCO}_3$  were close to equilibrium.

For the Buenavista stream segment, in samples S17, S18, S19, S20, and S20, carbonate compounds, such as siderite,  $\text{MgCO}_3$ ,  $\text{MnCO}_3$ , were subsaturated, as well as  $\text{SrSO}_4$ , while compounds  $\text{Ba}_3(\text{AsO}_4)_2$ ,  $\text{AlOOH}$  and  $\text{Zn}_2\text{SiO}_4$  were saturated.

The behaviors of the main reactive phases (aragonite, calcite, goethite, quartz, barite, and zincite) in the rainy season for the Taxco-Cocula sub-basin were like those of the dry season, except for samples S2 and S3; and other minerals were undersaturated or close to equilibrium.

Based on the results of this study, it is possible to affirm that the main geochemical process of AMD generation derives from the chemical oxidation of sulfides (especially pyrite). The process can be summarized in the following three steps: (1) pyrite oxidation in the presence of atmospheric oxygen and water is the main process generating acidity ( $\text{H}^+$ ) [44–47]. Usually, a decrease in pH is associated with an increase in TDS,  $\text{Fe}^{2+}$ , and  $\text{SO}_4^{2-}$ , which were documented in the areas studied [9,35]; (2) if the surrounding environment is sufficiently oxidizing, ferrous ion oxidizes to ferric ion and  $\text{Fe}^{3+}$  ions in solution can further oxidize additional pyrite and generate more acidity and release of  $\text{SO}_4^{2-}$  ions [44]; (3) hydrolysis and precipitation of ferric complexes, being chemical reactions producing most of the acidity in generation of the AMD process, generate three moles of  $\text{H}^+$  for one mole of pyrite [40,48]. The above does not consider the bacterial action that plays an important role in the oxidation process of  $\text{Fe}^{2+}$  to  $\text{Fe}^{3+}$  ions, based on sulfides. Chemolithotrophic bacteria act as catalysts, accelerating the oxidation process, decreasing pH and increasing ferric ion mobility in restricted environments [49–51].

The generation of secondary minerals, such as jarosite and hematite, releases protons and some metastable minerals transform into more stable phases, such as goethite, again producing protons and releasing sulfate ions [52,53]. Thus, hydroxide precipitation and hydrolysis are identified as part of the geochemical sequence of AMD production. If the pH is close to 2, ferric hydrolysis products, such as  $\text{Fe}(\text{OH})_3$ , are not stable and the  $\text{Fe}^{3+}$  ions remain in the solution [40]. Under these AMD conditions, minerals such as aluminosilicates can hydrolyze and release trivalent cations in the presence of aluminum in the main streams, evidenced by the high concentrations of HMs measured in the northern part of the recharge zone of the sub-basin (Figure 1).

The oxidation of MS-type minerals is responsible for the release of divalent metal and sulfate anions, without the production of acidity  $\text{MS} + 2\text{O}_2 = \text{M}^{2+} + \text{SO}_4^{2-}$  and, in the case of sphalerite, leach dissolved Zn and  $\text{SO}_4^{2-}$ , with variable amounts of Cd, while galena produces secondary anglesite ( $\text{PbSO}_4$ ) in equilibrium with a  $\text{Pb}^{2+}$  and  $\text{SO}_4^{2-}$  solution [28,40,47]. Thus, the oxidation of MS-type minerals in acidic environments releases water-soluble ions, as reported in this work (Tables S4 and S5, Supplementary Material).

The generation of AMD is a complex phenomenon that combines physical, chemical, and biological processes promoting the release and/or mobility of contaminants in restricted environments. Close to the tailings, such as at sampling site S2, there are no carbonate minerals (Tables S4 and S5) due to the low pH (<3.0). After sample S3, the pH value increased to circumneutral until sample S23.

The release of  $\text{H}^+$  in tailings depends on the number of minerals with the capacity to generate acidity, as well as minerals capable of neutralizing it, such as carbonates and silicates, which result in increase in pH from neutral to alkaline [40]. On the other hand, calcite is one of the most common carbonate minerals, with rapid neutralization capacity. As a result of neutralization processes, secondary minerals, such as gypsum, and Fe-Mn hydroxides, such as jarosite and goethite, are obtained, which also play important roles in buffering, acidification, and sorption processes that can seasonally retain HM mobility. Quevedo-Castañón et al. [35] reinforced the fact that the mobility of HMs in

the Xochula stream, where AMD originates (near S2), are mainly controlled by Fe and Mn oxyhydroxides, as well as by minerals, such as otavite, cuprousferrite, tenorite, and willemite, identified in this work. HM sorption and desorption reactions were identified by Méndez-Ramírez and Armienta Hernández [13] and Armienta et al. [33].

The processes described above justify the neutral to alkaline pH values in the main streams of the sub-basin. The buffering action of bicarbonate, the dilution of rainwater, the minerals forming the rocks, and the new secondary minerals, allow neutralization processes to take place. Therefore, acidic pH values were not reported beyond the S2 sampling point, where there were AMD generation processes.

The sorption and desorption reactions activated throughout the dry and rainy seasons are means of transport of HMs, due to the low energy of drag and decrease in the water flow in the dry season, favoring the deposition of sediments. Subsequently, the high drag energy in the rainy season erodes the particles and promotes movement of ions in the solution [35], and, thus, dispersion mechanisms are activated in each seasonal period.

The dispersion of HMs through these mechanisms leads to basin-wide concentrations in different proportions, as shown in this work, so that chemical processes of dissolution, oxidation, hydration, hydrolysis, neutralization, precipitation, sorption, and desorption can take place at the same time at different scales and at different locations.

Hydrogeological components, such as climate, topography, geology, and geomorphological features, determine the energy available for water movement in streams. Therefore, the chemical, physical and kinetic processes activated in each season could continue to act along the main river and a decrease in pollution could be reflected in the medium or long term. The result of this research shows the distribution of the spatial and temporal changes of mining origin contaminants along the Taxco-Cocula sub-basin.

## 5. Conclusions

The quality of water resources is characterized by the socioeconomic activities taking place within the studied sub-basin, and other main components are water–rock interactions, geological–mineralogical properties, the genesis of the mining deposits and the process of mineral exploitation. The springs analyzed had not been affected by mining activities, so their hydrochemical characteristics represent the natural presence of elements associated with the water's interaction with rocks. On the other hand, based on Mexican Standard NOM-127-SSA1-2021 and the regulations established by the WHO, the high concentrations of  $\text{SO}_4^{2-}$  and HM recorded in streams and the Taxco River, reflect poor quality [ $\text{SO}_4^{2-}$  (2600), Al (28.63), As (0.60), Cd (1.78), Cu (1.10), Fe (68.27), Mn (21.47), Pb (0.02), and Zn (208.80) in mg/L]. According to the concentrations of total metals measured in surface water, one can confirm that the main source of contamination derives from the Xochula stream (S2), located to the north in the recharge area at the sub-basin. Although the geology of the zone contributes to neutralizing the AMD, its process is not enough to avoid HM dispersion. Moreover, the tributary streams of Cacalotenango (S4, S5, S6, and S7) and Poza del Burro (S17, S18, and 19) contribute, to a lesser extent, to the concentrations of Al, As, Fe, and Zn originating from waste tailings. The Temixco stream (S9), El Sabinito (S13), the Los sabinos River (S15) and the San Juan River do not contribute to HM pollution through the sub-basin by themselves, but, nevertheless, they play a crucial role as transporting and diluent agents when they reach the Taxco River.

The measured HM concentrations in this study show the seasonal influences and the dispersion of HMs over the entire Taxco-Cocula sub-basin. In the dry season, oxidation, precipitation, and concentration processes act within the water system, whereas in the rainy season dilution, erosion, and deposition determine the transport of metals in surface water. The mechanisms involved in the dispersion of pollutants are activated in each season. Additionally, hydrogeological components, such as geology, climate, and topography, contribute to the dispersion of HMs along the main tributary of the Taxco-Cocula sub-basin.

**Supplementary Materials:** The following supporting information can be downloaded at: <https://www.mdpi.com/article/10.3390/w15101950/s1>, Table S1: Statistical values of major and minor ions measured in surface and ground water from Taxco-Cocula hydrological sub-basin; Table S2: Statistical values of heavy metals measured in surface and ground water from Taxco-Cocula hydrological sub-basin; Table S3: Multivariate analysis by using Principal Component Analysis; Table S4: Diversity of chemical reactive phases in the surface water of Taxco-Cocula sub-basin in dry season; Table S5: Diversity of chemical reactive phases in the surface water of Taxco-Cocula sub-basin in rainy season.

**Author Contributions:** J.C.R.-J. participated in the manuscript's investigation, and conceptualization; A.H.R.-G. participated in the manuscript's investigation, supervision, visualization, original draft writing, review, and editing; G.H.-F. participated in the manuscript's investigation, manuscript's supervision, conceptualization, visualization, original draft writing, review, and editing; M.A.H.H. participated in the manuscript's supervision, conceptualization, visualization, and original draft writing; O.T.-M. participated in the manuscript's investigation, supervision, and visualization; S.A.S.S. and A.C.-S. participated in the manuscript's investigation, supervision, visualization, original draft writing, and review. All authors have read and agreed to the published version of the manuscript.

**Funding:** This research received no external funding.

**Data Availability Statement:** All data presented in this study are contained within the article.

**Acknowledgments:** This research was carried out within the framework of the CONACYT grant awarded to Juan Carlos Ramírez Javier. The authors thank the CONACYT's Investigadores por México program, the Autonomous University of Guerrero, and the National University of Mexico.

**Conflicts of Interest:** The authors declare no conflict of interest. Also, the funders had no role in the design of the study; in the collection, analyses, or interpretation of data; in the writing of the manuscript; or in the decision to publish the results.

## References

1. Salvarredy-Aranguren, M.M.; Probst, A.; Roulet, M.; Isaure, M.-P. Contamination of surface waters by mining wastes in the Milluni Valley (Cordillera Real, Bolivia): Mineralogical and hydrological influences. *Appl. Geochem.* **2008**, *23*, 1299–1324. [[CrossRef](#)]
2. Sarmiento, A.M.; Nieto, J.M.; Olías, M.; Cánovas, C.R. Hydrochemical characteristics and seasonal influence on the pollution by acid mine drainage in the Odiel river Basin (SW Spain). *Appl. Geochem.* **2009**, *24*, 697–714. [[CrossRef](#)]
3. Mendoza, O.T.; Ruiz, J.; Villaseñor, E.D.; Guzmán, A.R.; Cortés, A.; Souto, S.A.S.; Almazán, A.D.; Bustos, R.R. Water-rock-tailings interactions and sources of sulfur and metals in the subtropical mining region of Taxco, Guerrero (southern Mexico): A multi-isotopic approach. *Appl. Geochem.* **2016**, *66*, 73–81. [[CrossRef](#)]
4. Atibu, E.K.; Lacroix, P.; Sivalingam, P.; Ray, N.; Giuliani, G.; Mulaji, C.K.; Otamonga, J.-P.; Mpiana, P.T.; Slaveykova, V.; Poté, J. High contamination in the areas surrounding abandoned mines and mining activities: An impact assessment of the Dilala, Luilu and Mpingiri Rivers, Democratic Republic of the Congo. *Chemosphere* **2018**, *191*, 1008–1020. [[CrossRef](#)]
5. Krauskopf, K.B.; Bird, D.K. *Introduction to Geochemistry*, 3rd ed.; McGraw-Hill: New York, NY, USA, 2003.
6. Chai, N.; Yi, X.; Xiao, J.; Liu, T.; Liu, Y.; Deng, L.; Jin, Z. Spatiotemporal variations, sources, water quality and health risk assessment of trace elements in the Fen River. *Sci. Total Environ.* **2021**, *757*, 143882. [[CrossRef](#)] [[PubMed](#)]
7. Wei, X.; Zhou, Y.; Jiang, Y.; Tsang, D.C.; Zhang, C.; Liu, J.; Zhou, Y.; Yin, M.; Wang, J.; Shen, N.; et al. Health risks of metal(loid)s in maize (*Zea mays* L.) in an artisanal zinc smelting zone and source fingerprinting by lead isotope. *Sci. Total Environ.* **2020**, *742*, 140321. [[CrossRef](#)]
8. Panamá, J.L.F.; Camprubí, A.; González-Partida, E.; Iriondo, A.; Gonzalez-Torres, E. Geochronology of Mexican mineral deposits. III: The Taxco epithermal deposits, Guerrero. *Bol. Soc. Geol. Mex.* **2015**, *67*, 357–366. [[CrossRef](#)]
9. Mendoza, O.T.; Yta, M.; Tovar, R.M.; Almazán, A.D.; Mundo, N.F.; Gutiérrez, C.D. Mineralogy and geochemistry of sulfide-bearing tailings from silver mines in the Taxco, Mexico area to evaluate their potential environmental impact. *Geofis. Int.* **2005**, *44*, 49–64. [[CrossRef](#)]
10. Mendoza, O.T.; Hernández, M.A.A.; Abundis, J.G.; Mundo, N.F. Geochemistry of leachates from the El Fraile sulfide tailings piles in Taxco, Guerrero, southern Mexico. *Environ. Geochem. Health* **2006**, *28*, 243–255. [[CrossRef](#)]
11. Vélez-Pérez, L.; Ramírez-Nava, J.; Hernández-Flores, G.; Talavera-Mendoza, O.; Escamilla-Alvarado, C.; Poggi-Varaldo, H.; Solorza-Feria, O.; López-Díaz, J. Industrial acid mine drainage and municipal wastewater co-treatment by dual-chamber microbial fuel cells. *Int. J. Hydrogen Energy* **2020**, *45*, 13757–13766. [[CrossRef](#)]
12. Arcega-Cabrera, F.; Armienta, M.; Daesslé, L.; Castillo-Blum, S.; Talavera, O.; Dótor, A. Variations of Pb in a mine-impacted tropical river, Taxco, Mexico: Use of geochemical, isotopic and statistical tools. *Appl. Geochem.* **2009**, *24*, 162–171. [[CrossRef](#)]
13. Méndez-Ramírez, M.; Armienta Hernández, M.A. Distribución de Fe, Zn, Pb, Cu, Cd y As originada por residuos mineros y aguas residuales en un transecto del Río Taxco en Guerrero, México. *Rev. Mex. de Cienc. Geol.* **2012**, *29*, 450–462.

14. Ramírez Javier, J.C. Dispersión de Elementos Potencialmente Tóxicos e Influencia Estacional en Una Subcuenca Hidrológica Con Influencia Minera al Norte del Estado de Guerrero. Master's Thesis, Universidad Autónoma de Guerrero, Acapulco, Mexico, 2019; p. 74.
15. DOF (Diario Oficial de la Federación). *Modificación de la Norma Oficial Mexicana NOM-127-SSA1-2021, Agua Para Uso y Consumo Humano. Límites Permisibles de la Calidad del Agua*. Secretaría de Salud; Diario Oficial de la Federación: Mexico City, Mexico, 2022.
16. WHO (World Health Organization). *Guidelines for Drinking Water Quality*, 4th ed.; WHO: Geneva, Switzerland, 2011.
17. Campa-Uranga, M.F.; Torres-de León, R.; Iriondo, A.; Wayne, R.P. Caracterización geológica de los ensambles metamórficos de Taxco y Taxco el Viejo, Guerrero, México. *Bol. Soc. Geol. Mex.* **2012**, *64*, 369–385. [[CrossRef](#)]
18. Morán-Zenteno, D.; Alba-Aldave, L.; Solé, J.; Iriondo, A. A major resurgent caldera in southern Mexico: The source of the late Eocene Tilzapotla ignimbrite. *J. Volcanol. Geotherm. Res.* **2004**, *136*, 97–119. [[CrossRef](#)]
19. Omaña-Pulido, L.; Alencáster-Ybarra, G. Lower Aptian shallow-water benthic foraminiferal assemblage from the Chilacachapa range in the Guerrero-Morelos Platform, south Mexico. *Rev. Mex. Cienc. Geol.* **2009**, *26*, 575–586.
20. Cerca-Martínez, M. Deformación y Magmatismo CRETÁCICO Tardío—Terciario Temprano en la Zona de la Plataforma Guerrero Morelos. Ph.D. Thesis, Centro de Geociencias, Campus UNAM Juriquilla, Juriquilla, Mexico, 2004.
21. Perrilliat-Montoya, M.C.; Vega-Vera, F.J.; Corona-Esquivel, R.J. Early Maastrichtian mollusca from the Mexcala Formation of the state of Guerrero, Southern Mexico. *J. Paleontol.* **2000**, *74*, 7–24. [[CrossRef](#)]
22. Alaniz-Álvarez, S.; Nieto-Samaniego, A.; Morán-Zenteno, D.; Alba-Aldave, L.A. Rhyolitic volcanism in extension zone associated with strike-slip tectonics in the Taxco region, southern Mexico. *J. Volcanol. Geotherm. Res.* **2002**, *118*, 1–14. [[CrossRef](#)]
23. Guerrero-Suástegui, M. Depositional and Tectonic History of The Guerrero Terrane, Sierra Madre del Sur; with Emphasis on Sedimentary Successions of the Teloloapan Area, Southwestern Mexico. Ph.D. Thesis, University of Newfoundland, St. John's, NL, Canada, 2004; 332p.
24. Comisión Nacional del Agua (CONAGUA). *Atlas del Agua en México 2015*; Secretaría de Medio Ambiente y Recursos Naturales: Mexico City, Mexico, 2015; 135p.
25. Comisión Nacional del Agua (CONAGUA). *Estadísticas del Agua en la Cuenca del Río Balsas 2010*; Secretaría de Medio Ambiente y Recursos Naturales; Organismo de Cuenca Balsas: Mexico City, Mexico, 2010; 170p.
26. Sánchez-Montoya, G.; Talavera-Mendoza, O.; Hernández-Flores, G.; Díaz-Villaseñor, E.; Ramírez-Guzmán, A.H.; Galarza-Brito, Z. Potentially toxic elements determination and chemical-microbiological analysis of potable water in Taxco de Alarcón, Guerrero. *Rev. Mex. Cienc. Geol.* **2019**, *36*, 147–158. [[CrossRef](#)]
27. Camprubí, A.; González-Partida, E.; Torres-Tafolla, E. Fluid inclusion and stable isotope study of the Cobre–Babilonia polymetallic epithermal vein system, Taxco district, Guerrero, Mexico. *J. Geochem. Explor.* **2006**, *89*, 33–38. [[CrossRef](#)]
28. Romero, F.; Armienta, M.; González-Hernández, G. Solid-phase control on the mobility of potentially toxic elements in an abandoned lead/zinc mine tailings impoundment, Taxco, Mexico. *Appl. Geochem.* **2007**, *22*, 109–127. [[CrossRef](#)]
29. Gallagher, D.; Pérez-Siliceo, R.P. *Geology of the Huahuaxtla Mercury District, State of Guerrero, Mexico*; U.S. Geological Survey: Reston, VA, USA, 1948; pp. 149–175. [[CrossRef](#)]
30. Servicio Geológico Mexicano (SGM). *Carta Geológico-Minero E14A68 Guerrero y Morelos*; Primera edición marzo del 2004; Secretaria de Economía: Mexico City, Mexico, 2004.
31. APHA; AWWA; WEF. *Standard Methods for the Examination Water and Wastewater*, 21st ed.; APHA; AWWA; WEF: Washington, DC, USA, 2005.
32. Parkhurst, D.L.; Appelo, C.A.J. *User Guide to PHREEQC a Computer Program for Speciation, Reaction-Path, ID Transport, and Inverse Geochemical Calculations*; Water-Resources Investigations Report 95-4227; United States Geological Survey: Reston, VA, USA, 1999; 312p.
33. Armienta, M.A.; Talavera, O.; Villaseñor, G.; Espinosa, E.; Pérez-Martínez, I.; Cruz, O.; Cenicerros, N.; Aguayo, A. Environmental behaviour of metals from tailings in shallow rivers: Taxco, central Mexico. *Appl. Earth Sci.* **2004**, *113*, 76–82. [[CrossRef](#)]
34. Armienta, M.A.; Talavera, O.; Morton, O.; Barrera, M. Geochemistry of Metals from Mine Tailings in Taxco, Mexico. *Bull. Environ. Contam. Toxicol.* **2003**, *71*, 387–393. [[CrossRef](#)] [[PubMed](#)]
35. Quevedo-Castañón, N.M.; Mendoza, O.T.; Salgado-Souto, S.A.; Ruiz, J.; Dótor-Almazán, A.; Ramírez-Guzmán, A.H.; Sampedro-Rosas, L.; Rosas-Acevedo, J.L.; Chávez-González, J.D. Temporal and spatial hydrogeochemical evolution and lead isotopic composition of a contaminated stream of Taxco, Guerrero, Mexico. *Rev. Mex. Cienc. Geol.* **2020**, *37*, 64–79. [[CrossRef](#)]
36. Martínez-Castrejón, M.; Ramirez-Nava, J.; López-Díaz, J.A.; Talavera-Mendoza, O.; García-Mesino, R.L.; Salgado-Souto, S.A.; Ramírez-Guzmán, A.H.; Sarmiento-Villagrana, A.; Hernández-Flores, G. Acid mine drainage treatment using chicken eggshell waste. *Rev. Int. Contam. Ambie.* **2022**, *38*, 431–447. [[CrossRef](#)]
37. Xiao, J.; Lv, G.; Chai, N.; Hu, J.; Jin, Z. Hydrochemistry and source apportionment of boron, sulfate, and nitrate in the Fen River, a typical loess covered area in the eastern Chinese Loess Plateau. *Environ. Res.* **2022**, *206*, 112570. [[CrossRef](#)]
38. Tóth, J. Groundwater as a geologic agent: An overview of the causes, processes, and manifestations. *Hydrogeol. J.* **1999**, *7*, 1–14. [[CrossRef](#)]
39. Banks, D.; Younger, P.L.; Arnesen, R.-T.; Iversen, E.R.; Banks, S.B. Mine-water chemistry: The good, the bad and the ugly. *Environ. Geol.* **1997**, *32*, 157–174. [[CrossRef](#)]
40. Dold, B. Basic Concepts in Environmental Geochemistry of Sulfidic Mine-Waste Management. In *Waste Management*; Kumar, E.S., Ed.; InTech: London, UK, 2010; pp. 174–198, ISBN 978-953-7619-84-8.

41. Sherlock, E.J.; Lawrence, R.W.; Poulin, R. On the neutralization of acid rock drainage by carbonate and silicate minerals. *Environ. Geol.* **1995**, *25*, 43–54. [[CrossRef](#)]
42. Appelo, C.A.J.; Postma, D. *Geochemistry, Groundwater and Pollution*, 2nd ed.; A. A. Balkema Publishers: Leiden, The Netherlands, 2005; p. 683.
43. Romero, F.M.; Núñez, L.; Gutiérrez, M.E.; Armienta, M.A.; Cenicerós-Gómez, A.E. Evaluation of the Potential of Indigenous Calcareous Shale for Neutralization and Removal of Arsenic and Heavy Metals from Acid Mine Drainage in the Taxco Mining Area, Mexico. *Arch. Environ. Contam. Toxicol.* **2011**, *60*, 191–203. [[CrossRef](#)]
44. Blowes, D.W.; Jambor, J.L.; Hanton-Fong, C.J.; Lortie, L.; Gould, W. Geochemical, mineralogical and microbiological characterization of a sulphide-bearing carbonate-rich gold-mine tailings impoundment, Joutel, Québec. *Appl. Geochem.* **1998**, *13*, 687–705. [[CrossRef](#)]
45. Jacobs, J.A.; Lehr, J.H.; Testa, S.M. *Acid Mine Drainage, Rock Drainage, and Acid Sulfate Soils: Causes, Assessment, Prediction, Prevention, and Remediation*; John Wiley & Sons: Hoboken, NJ, USA, 2014.
46. Jamieson, H.E.; Walker, S.R.; Parsons, M.B. Mineralogical characterization of mine waste. *Appl. Geochem.* **2015**, *57*, 85–105. [[CrossRef](#)]
47. Simate, G.S.; Ndlovu, S. Acid mine drainage: Challenges and opportunities. *J. Environ. Chem. Eng.* **2014**, *2*, 1785–1803. [[CrossRef](#)]
48. Dold, B.; Fontboté, L. Element cycling and secondary mineralogy in porphyry copper tailings as a function of climate, primary mineralogy, and mineral processing. *J. Geochem. Explor.* **2001**, *74*, 3–55. [[CrossRef](#)]
49. Bond, P.L.; Druschel, G.K.; Banfield, J.F. Comparison of Acid Mine Drainage Microbial Communities in Physically and Geochemically Distinct Ecosystems. *Appl. Environ. Microbiol.* **2000**, *66*, 4962–4971. [[CrossRef](#)]
50. Johnson, D.; Hallberg, K.B. The microbiology of acidic mine waters. *Res. Microbiol.* **2003**, *154*, 466–473. [[CrossRef](#)]
51. Nordstrom, D.K.; Blowes, D.W.; Ptacek, C.J. Hydrogeochemistry and microbiology of mine drainage: An update. *Appl. Geochem.* **2015**, *57*, 3–16. [[CrossRef](#)]
52. Acero, P.; Ayora, C.; Torrentó, C.; Nieto, J.-M. The behavior of trace elements during schwertmannite precipitation and subsequent transformation into goethite and jarosite. *Geochim. Cosmochim. Acta* **2006**, *70*, 4130–4139. [[CrossRef](#)]
53. Jönsson, J.; Jönsson, J.; Lövgren, L. Precipitation of secondary Fe(III) minerals from acid mine drainage. *Appl. Geochem.* **2006**, *21*, 437–445. [[CrossRef](#)]

**Disclaimer/Publisher’s Note:** The statements, opinions and data contained in all publications are solely those of the individual author(s) and contributor(s) and not of MDPI and/or the editor(s). MDPI and/or the editor(s) disclaim responsibility for any injury to people or property resulting from any ideas, methods, instructions or products referred to in the content.